

Electro-optomechanical equivalent circuits for quantum transduction

Emil Zeuthen,^{1,2,*} Albert Schliesser,¹ Jacob M. Taylor,^{3,4} and Anders S. Sørensen¹

¹*Niels Bohr Institute, University of Copenhagen, DK-2100 Copenhagen, Denmark*

²*Institute for Theoretical Physics and Institute for Gravitational Physics (Albert Einstein Institute), Leibniz Universität Hannover, Callinstraße 38, 30167 Hannover, Germany*

³*Joint Quantum Institute, University of Maryland/National Institute of Standards and Technology, College Park, Maryland 20742, USA*

⁴*Joint Center for Quantum Information and Computer Science, University of Maryland, College Park, Maryland 20742, USA*

Using the techniques of optomechanics, a high- Q mechanical oscillator may serve as a link between electromagnetic modes of vastly different frequencies. This approach has successfully been exploited for the frequency conversion of classical signals and has the potential of performing quantum state transfer between superconducting circuitry and a traveling optical signal. Such transducers are often operated in a linear regime, where the hybrid system can be described using linear response theory based on the Heisenberg-Langevin equations. While mathematically straightforward to solve, this approach yields little intuition about the dynamics of the hybrid system to aid the optimization of the transducer. As an analysis and design tool for such electro-optomechanical transducers, we introduce an equivalent circuit formalism, where the entire transducer is represented by an electrical circuit. Thereby we integrate the transduction functionality of optomechanical (OM) systems into the toolbox of electrical engineering allowing the use of its well-established design techniques. This unifying impedance description can be applied both for static (DC) and harmonically varying (AC) drive fields, accommodates arbitrary linear circuits, and is not restricted to the resolved-sideband regime. Furthermore, by establishing the quantized input/output formalism for the equivalent circuit, we obtain the scattering matrix for linear transducers using circuit analysis, and thereby have a complete quantum mechanical characterization of the transducer. Hence, this mapping of the entire transducer to the language of electrical engineering both sheds light on how the transducer performs and can at the same time be used to optimize its performance by aiding the design of a suitable electrical circuit.

CONTENTS

I. Introduction	2
A. Equivalent circuits	3
B. Structure of paper	4
II. Electromechanical interfaces	4
A. Parametric electro-mechanical coupling	4
B. Enhanced linearized interaction in presence of a drive field	5
III. Intuitive derivation of electromechanical equivalent circuit for DC bias	6
A. Dynamical variables of the equivalent circuit	6
B. Effective mechanical resonance frequencies	8
IV. Electromechanical equivalent circuit for AC drive	8
V. Electrical input-output formalism	11
VI. Quantization of the equivalent circuit	14
VII. Optical impedance and full electro-optomechanical equivalent circuit	15
VIII. Example of application	20
IX. Adiabatic elimination of electrical and optical modes	21

* zeuthen@nbi.ku.dk

A. Elimination of optical mode	22
B. Elimination of electrical modes	23
X. Conclusion and outlook	24
Acknowledgments	25
References	25

I. INTRODUCTION

Quantum-coherent technology is envisioned to usher in a new era of information processing and communication. While quantum effects are already at play in semiconductor transistors and lasers, quantum-coherent effects are believed to take center stage in future quantum technology. To implement this, the entire infrastructure must be built on quantum-enabled components, and this has spurred a wide-ranging research effort into, e.g., quantum processors (gates), quantum memory, quantum transistors, and quantum error correction. Quantum computers, built from such components, are envisioned to be securely networked via optical fibers [1] on account of their long-distance transmission capabilities, thereby forming a quantum internet [2]. Since several quantum computing architectures are working in the frequency domain of GHz, this poses the demand for a quantum “modem” providing a hookup to the optical network. Such a device should provide quantum-coherent frequency conversion, also referred to as *quantum transduction*, thereby bringing together the strengths of, e.g., on the one hand, superconducting circuitry in which quantum gates and state preparation can be performed efficiently and, on the other hand, the low-loss transmission and quantum-limited detection of optical signals. These advantageous features of the optical domain persist even at room temperature. Hence the successful transduction of low-frequency signals to the optical regime may also be exploited for the sensitive detection of weak, classical electrical signals.

Transduction typically involves a modulation mechanism. A strong and versatile candidate for such a mechanism can be found within optomechanics. This research field is concerned with the interaction between light fields and mechanical oscillators through the radiation pressure force [3, 4]. One can greatly enhance this force in a strongly driven high-finesse cavity. This idea has been realized over a very wide mass spectrum ranging from nanoscale objects to the macroscopic mirrors employed in gravitational wave detection [5]. With this approach, a new regime has been attained in the past decade in which the backaction of the light on the mechanical motion due to the radiation pressure force is significant [6–10]. Moreover, the availability of mechanical oscillators with quality factors in excess of 10^6 combined with cryogenic cooling allows quantum operation, where several mechanical oscillations can occur before a phonon is lost or a thermal phonon is added. This has enabled surprising levels of control with meso- and macroscopic mechanical oscillators allowing optical cooling of the mechanical motion to near its quantum-mechanical ground state [11–15].

Since electromagnetic fields from all parts of the spectrum can exert a force on mechanical objects, the principles of optomechanics find their complete analogs in the context of radio-frequency and microwave electrical circuits. Electromechanical transduction has been exploited in the classical regime since the advent of the telephone in the late 19th century. Paralleling the rapid development in optomechanics, experiments in the micro- and nanoelectromechanical (MEMS and NEMS) communities have also reached the quantum regime. Among the most notable achievements are cooling of a mechanical oscillator to the vicinity of its ground state [16–18], reversible state transfer of quantum-level signals between electromagnetic fields and a mechanical mode [19, 20], and mechanical microwave amplification [21–23] near the quantum limit.

Hence both optomechanics and electromechanics are mature research directions offering quantum-level operation. By combining the two, they would therefore offer a promising platform for quantum transduction between electrical and optical frequencies [24–28] allowing loss- and noise-less conversion of quantum states, but also the generation of, e.g., two-mode squeezed hybrid states of light and microwaves for continuous-variable teleportation [29] and entanglement between distant superconducting qubits by transducer-mediated interaction with a common propagating optical field [30]. In fact, optomechanical interfaces suitable for integration with electrical circuits have already been devised [31–43]. A prominent example of this is the Membrane-In-The-Middle optomechanical system in which a micromechanical membrane is placed inside a Fabry-Pérot cavity with fixed end mirrors [31]. This geometry allows significant freedom to simultaneously optimize optical and mechanical properties. Moreover, the fact that the mechanical degree of freedom does not involve the optical components permits easy integration with electrical systems. In particular, it can be directly incorporated into floating-electrode geometries [32], where a mechanically compliant dielectric or conductor moves in the quasi-electrostatic field of fixed electrodes, thereby modulating their capacitance [33]. Using this approach, electro-optomechanical hybrid devices have already been built where a me-

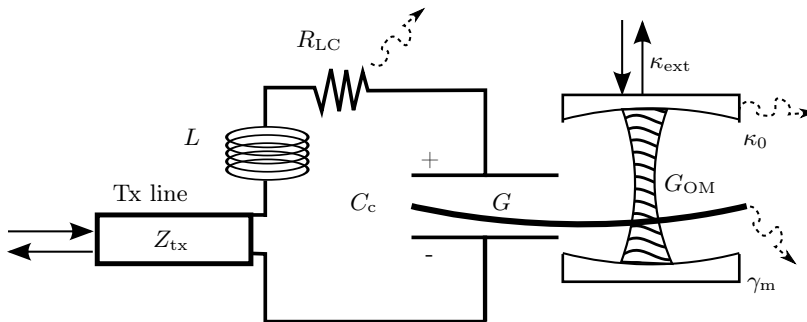


Figure 1. Example electro-optomechanical transducer: A serial RLC circuit with intrinsic resistance R_{LC} is loaded by a semi-infinite transmission line of characteristic impedance Z_{tx} . The circuit is capacitively coupled to a mechanical mode of intrinsic linewidth γ_m with coupling strength G . Analogously, the optical mode has an intrinsic loss rate κ_0 and a readout rate κ_{ext} and couples to the mechanical mode with strength G_{OM} .

chanical mode couples simultaneously to optical and electrical fields (see Fig. 1), thereby realizing optical readout of radio-frequency signals in a room-temperature electrical circuit [34, 43] as well as microwave-to-optical transduction in setups designed for cryogenic operation [35, 36, 38]. Alternatively, the electromechanical coupling can be implemented piezoelectrically [39–42].

Electro-optomechanics brings together the research fields of electrical engineering and quantum optics, both of which have a well-developed set of experimental and theoretical tools. To realize the full potential of marrying these two fields it is highly desirable to establish a common language for the resulting hybrid systems, thus making the knowledge and techniques from one system applicable to the other.

A. Equivalent circuits

In this article, we develop an equivalent circuit formalism for electro-optomechanical transducers that accommodates arbitrary linear electrical circuits. With this approach the entire coupled system of electrical modes, mechanical vibrations, and optical fields can be described in terms of a linear electrical circuit obeying Kirchhoff's laws. We consider the system shown in Fig. 2(a), where a membrane is inserted into a capacitor such that the capacitance $C_c(x)$ depends on the excursion x of the membrane from its equilibrium position. When the membrane moves it thereby modulates the capacitance, which leads to a coupling of the mechanical motion and the electric circuit. We show that in the linear regime this system can be exactly represented by the electrical circuit in Fig. 2(b). Here the mechanical oscillator is represented by a parallel arm containing an RLC circuit with resonance frequency and damping set by the corresponding mechanical parameters. The position of the membrane x is then directly related to the charge δQ_m sitting on the capacitor in the parallel arm, $x \propto \delta Q_m$. The formal reason that such an equivalent-circuit formulation is possible, is that all the involved systems are conveniently described in the Heisenberg-Langevin input-output formalism for coupled oscillators [44, 45]. For an arbitrary linear circuit, the Heisenberg-Langevin equations are nothing but a quantized version of Kirchhoff's well-known circuit laws [46]. As a consequence, all the involved degrees of freedom can be mapped to electrical analogs thereby allowing a common equivalent circuit description of the full electro-optomechanical system. Hence, one may adequately describe the system by Kirchhoff's laws with impedances determined by the electro-optomechanical couplings.

A similar representation of mechanical oscillation modes coupled to an electrical circuit by an equivalent circuit element is already an established tool in the MEMS community [47, 48], known as the Butterworth-van Dyke circuit, and has also been applied in the contexts of cavity-electromechanics [49] and piezo crystals [16]. We take this idea further by making the following important extensions: Firstly, we derive a quite general, yet simple, equivalent circuit for AC-driven electromechanical (EM) systems as is typical of experiments in the microwave domain. Secondly, we derive the impedance of a mechanically coupled optical mode in a high-finesse optical resonator, allowing us to construct a full electro-optomechanical equivalent circuit. Moreover, we will discuss how to quantize the theory.

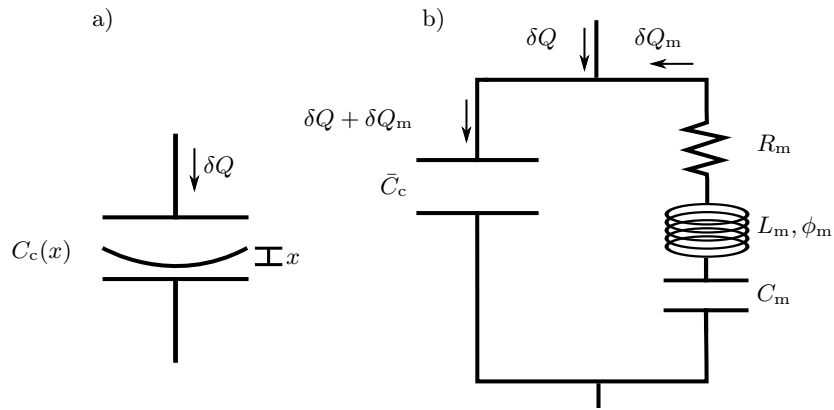


Figure 2. a) Sketch of a mechanically modulated coupling capacitor, $C_c(x)$, where x is a suitable mechanical position coordinate and δQ is an added charge. b) Equivalent circuit model for the system in a) in which the mechanical mode is represented by a serial RLC circuit in parallel to the *unmodulated* coupling capacitor \bar{C}_c . The charge δQ_m and the magnetic flux ϕ_m play the roles of position and momentum, respectively. The equivalent mechanical resistance R_m , inductance L_m , and capacitance C_m correspond to damping rate, mass, and (inverse) spring constant, respectively.

B. Structure of paper

We will establish the electro-optomechanical equivalent circuit formalism in the following steps: First we introduce a Hamiltonian description for EM interfaces in Section II; based on this, we give an intuitive derivation of the mechanical equivalent impedance for a DC-biased interface in Section III. Next, we extend the EM equivalent circuit to the case of an AC electrical drive in Section IV. Then, in Section V, we supplement the impedance formalism by introducing electrical input-output theory, which allows us to consider the in- and outcoupling of signals and noise. Based on this, we describe how to quantize the theory in Section VI and demonstrate the formalism by calculating the squeezing spectrum of a simple electromechanical system using standard rules for combining impedances. Having established all aspects of the EM equivalent circuit, we then introduce the optical subsystem by analogy in Section VII, thereby arriving at the full electro-optomechanical equivalent circuit. As an example of the application of the formalism, we apply it to a simple transducer in Section VIII. In Section IX we derive a reduced equivalent circuit by adiabatic elimination of the electrical and optical modes. Finally, we conclude and give an outlook in Section X.

II. ELECTROMECHANICAL INTERFACES

In this section we will introduce a Hamiltonian description for capacitive EM coupling and discuss the linearization of the interaction around the steady-state configuration induced by the drive field.

A. Parametric electro-mechanical coupling

We consider a single viscously damped mechanical mode with canonical position x and momentum p , whose evolution is governed by the Langevin equations (in the absence of EM coupling),

$$\begin{aligned} \dot{x} &= p/m \\ \dot{p} &= -m\omega_{m,0}^2 x - \gamma_{m,0} p + F(t), \end{aligned} \quad (1)$$

where dot signifies the time derivative, m is the mass, $\omega_{m,0}$ is the resonance frequency, $\gamma_{m,0}$ is the damping rate and F is the associated stochastic force, whose fluctuation spectrum is [50]

$$\langle F^*(\omega) F(\omega') \rangle = 2m\gamma_{m,0} k_B T_m \delta(\omega - \omega'), \quad (2)$$

where k_B is Boltzmann's constant and T_m is the ambient temperature of the mechanical component. The classical Eqs. (1,2) represent the high-temperature limit ($k_B T_m \gg \hbar\omega_{m,0}$) of quantum Brownian motion, which is governed by

Eq. (1) with x , p , and F elevated to operators, and the fluctuation spectrum (2) generalized to $(\omega, \omega' > 0)$ [51]

$$\begin{aligned}\langle \hat{F}^\dagger(\omega) \hat{F}(\omega') \rangle &= 2m\gamma_{m,0} \hbar \omega n_m(\omega) \delta(\omega - \omega'), \\ \langle \hat{F}(\omega) \hat{F}^\dagger(\omega') \rangle &= 2m\gamma_{m,0} \hbar \omega [n_m(\omega) + 1] \delta(\omega - \omega'),\end{aligned}\quad (3)$$

in terms of the Bose-Einstein distribution,

$$n_i(\omega) \equiv (e^{\hbar\omega/(k_B T_i)} - 1)^{-1}. \quad (4)$$

For later reference we note that the mechanical evolution (1) derives from the (classical) Hamiltonian

$$H_{m,0} = \frac{p^2}{2m} + \frac{1}{2} m \omega_{m,0}^2 x^2, \quad (5)$$

plus additional terms accounting for the coupling to the bath responsible for the damping and noise fluctuations.

In order to construct an EM transducer it is essential to have a coupling between the mechanical and electronic degrees of freedom. Motivated by recent experiments [17, 19, 34, 35, 52], we will consider a capacitive coupling where the mechanical oscillator modulates the capacitance C_c of a capacitor in the circuit such that it acquires a dependence on the mechanical position, $C_c(x)$, see Fig. 2a. The physical mechanism underlying this dependence depends on the implementation, but examples include the Kelvin polarization force from an inhomogeneous electric field on a dielectric mechanical element [32, 53] and the quasi-electrostatic interaction with a conductive mechanical element [17, 18, 33, 52, 54], but the precise nature of the coupling is not important for this study (e.g., the formalism developed below for the linearized dynamics can also be extended to inductive [55] or piezoelectric [16, 39] coupling). Since the motion of the mechanical oscillator modulates the capacitance it also modulates the resonance frequency of the circuit, thus giving rise to a dispersive interaction. As an alternative to this, other types of coupling have been proposed including dissipative coupling [56] and mechanical multimode schemes [52, 57, 58]. Here we restrict ourselves to the capacitive coupling, but the formalism is likely to be extendable to accommodate other kinds of parametric couplings as well as multiple mechanical modes.

If a charge Q is added to the capacitor, the dependence of the capacitance on the position means that there is a force on the mechanical oscillator which will displace it to a new equilibrium value \bar{x} . Here we are interested in the small fluctuations $\delta x \equiv x - \bar{x}$ around this equilibrium. We therefore expand the charging energy of the capacitor to obtain

$$H_C = \frac{Q^2}{2C_c(x)} \approx \frac{Q^2}{2\bar{C}_c} - \frac{1}{2} \frac{Q^2}{\bar{C}_c^2} \left. \frac{dC_c}{dx} \right|_{x=\bar{x}} \delta x + \frac{Q^2}{4\bar{C}_c^2} \left[\frac{2}{\bar{C}_c} \left(\left. \frac{dC_c}{dx} \right|_{x=\bar{x}} \right)^2 - \left. \frac{d^2 C_c}{dx^2} \right|_{x=\bar{x}} \right] \delta x^2, \quad (6)$$

where $\bar{C}_c \equiv C_c(\bar{x})$ denotes the steady-state value of the coupling capacitance. Note, that the notion of a position-dependent charging energy, presumed in Eq. (6), is only meaningful in the quasi-electrostatic limit, where the charges on the capacitive element equilibrates much faster than the timescale of the mechanical modulation $2\pi/\omega_{m,0}$.

B. Enhanced linearized interaction in presence of a drive field

The EM interaction Hamiltonian (6) is non-linear in nature and typically very weak. For transduction, however, linear interaction is typically sufficient and even desirable. A much stronger interaction can then be obtained by applying a strong classical drive voltage which induces a charge $\bar{Q}_c(t)$ of large amplitude on the capacitor. Such biasing is a well-known technique in electronics, e.g., it is the operating principle behind condenser microphones, in which one plate of a capacitor is a diaphragm susceptible to sound waves. We will consider two different situations: If the electrical signal is near resonance with the mechanical oscillator a DC bias is sufficient to couple the two, whereas if they are different an AC bias is required to bridge the difference in resonance frequencies. As for the position variable above, we are interested in the small charge fluctuations δQ around the mean and make the replacement $Q \rightarrow \bar{Q}_c(t) + \delta Q$. We can then derive the effective Hamiltonian governing the interactions among the fluctuation variables $\delta x, \delta Q$. For simplicity, we assume a monochromatic electrical drive and, moreover, that the circuit responds linearly, so as to induce a fluctuating charge on the coupling capacitor

$$\bar{Q}_c(t) = \begin{cases} \bar{Q}_{c,0} e^{i\omega_a t} + \bar{Q}_{c,0}^* e^{-i\omega_a t} & \text{[AC drive]} \\ \bar{Q}_{c,0} & \text{[DC bias]} \end{cases}, \quad (7)$$

where in the case of DC bias $\bar{Q}_{c,0}$ must be real. With this charge bias, Eq. (6) leads to a linear interaction among the fluctuation variables to lowest order,

$$H_{\text{EM,int}} \approx -\frac{\bar{Q}_c(t)}{\bar{C}_c^2} \frac{dC_c}{dx} \Big|_{x=\bar{x}} \delta Q \delta x = \delta Q \delta x \times \begin{cases} G e^{i\omega_d t} + G^* e^{-i\omega_d t} & \text{[AC drive]} \\ G & \text{[DC bias]} \end{cases}. \quad (8)$$

Here we have introduced the drive-enhanced EM coupling parameter G (SI units of V/m):

$$G \equiv -\frac{\bar{Q}_{c,0}}{\bar{C}_c^2} \frac{dC_c}{dx} \Big|_{x=\bar{x}}. \quad (9)$$

Throughout this article we attempt to emphasize both the similarities and differences between the DC- and AC-biased EM interfaces. Eq. (7) implies that in the AC-driven case we define $|\bar{Q}_{c,0}|$ to be half of the charge amplitude whereas in the DC case it is the full amplitude; this choice allows for a simpler presentation below. The EM coupling strength G introduced in Eq. (9) will play a central role in the derivation of the equivalent picture later on as it characterizes the strength of the interaction. A related, more familiar parameter in the optomechanics community is the linearized coupling rate g_{EM} between the two bosonic modes representing the circuit and mechanical resonances (as will be detailed below in Section VII for the equivalent OM case). An advantage of G over g_{EM} is that the former can be meaningfully defined without specifying an electrical circuit resonance and therefore we will focus on G in the derivation below.

III. INTUITIVE DERIVATION OF ELECTROMECHANICAL EQUIVALENT CIRCUIT FOR DC BIAS

We will now give a simple derivation of the equivalent circuit representation of an optomechanical system coupled to an electrical circuit. For simplicity we start with the case of DC-biased EM coupling, postponing the AC-driven scenario until Section IV. In essence, we are looking for a way to describe the linear response of the system depicted in Fig. 2a with a circuit diagram consisting of standard components (capacitors, inductors, etc.). In the figure only the coupling capacitor is drawn, but it is assumed to be connected to an arbitrary linear circuit. Assume that we add a positive charge δQ to the positive equilibrium charge $\bar{Q}_{c,0}$ already present on the EM capacitor of capacitance $C_c(x = \bar{x})$. In this case the additional charge will introduce a force on the oscillator which pushes it towards a larger capacitance (so that $x = \bar{x} + \delta x$) in order to reduce the charging energy. As a consequence, the voltage fluctuation induced on the capacitor $\delta V(x)$ will be smaller than anticipated from the naive expectation $\delta V(\bar{x}) = \delta Q / C_c(\bar{x})$. Instead of modeling this as a capacitance which depends on δx we instead introduce a fixed capacitance $\bar{C}_c \equiv C_c(\bar{x})$ and model the reduced voltage fluctuations as being due to a part of the charge $-\delta Q_m$ not sitting on the capacitor but instead being diverted to an equivalent *mechanical* circuit branch *in parallel* to the coupling capacitor as shown in Fig. 2b [48]. Seen from the outside, the voltage fluctuation δV on the capacitor will be exactly the same if we chose a suitable δQ_m , and hence the two systems are equivalent. Since the charge diverted to the parallel mechanical arm represents the mechanical motion, $\delta Q_m \propto \delta x$, we expect it to obey similar equations of motion as the viscously damped harmonic oscillator (1). Such an oscillator is mathematically equivalent to a serial RLC circuit and we therefore expect the mechanical arm to be simply a serial RLC circuit,

$$Z_m(\omega) = -i\omega L_m + R_m + \frac{1}{-i\omega C_m}, \quad (10)$$

where L_m , R_m , and C_m are mechanical equivalent circuit parameters (see Fig. 2b). Below we confirm this ansatz for the mechanical impedance $Z_m(\omega)$ and derive explicit expressions for the individual components in terms of the known physical parameters.

A. Dynamical variables of the equivalent circuit

To derive the equivalent mechanical circuit, we consider the linearized Hamiltonian describing the mechanical system and the coupling capacitor

$$H_C + H_{m,0} \approx \frac{\delta Q^2}{2\bar{C}_c} + \frac{1}{2} m \omega_{m,Q}^2 \delta x^2 + \frac{p^2}{2m} + G \delta Q \delta x, \quad (11)$$

from Eqs. (5,6). Here we have defined a modified mechanical frequency $\omega_{m,Q}$ including the second order derivative in Eq. (6)

$$\omega_{m,Q}^2 = \omega_{m,0}^2 + \frac{\bar{C}_c G^2}{m} - \frac{\langle \bar{Q}_c^2(t) \rangle}{2m\bar{C}_c^2} \frac{d^2 C_c}{dx^2} \Big|_{x=\bar{x}}. \quad [\text{DC bias}] \quad (12)$$

The precise interpretation of this frequency will be discussed below. Note that we have introduced the time average $\langle \cdot \rangle$ of the square of the bias charge for consistency with the AC driven case discussed below. For the DC-biased case this is simply given by $\langle \bar{Q}_c^2(t) \rangle = \bar{Q}_{c,0}^2$.

The aim is now to see whether the system can be mapped to the equivalent circuit shown in Fig. 2b. The (non-dissipative) Hamiltonian corresponding to this circuit is

$$\begin{aligned} H' &= \frac{(\delta Q + \delta Q_m)^2}{2\bar{C}_c} + \frac{\delta Q_m^2}{2C_m} + \frac{\phi_m^2}{2L_m} \\ &= \frac{\delta Q^2}{2\bar{C}_c} + \frac{1}{2} \left(\frac{1}{\bar{C}_c} + \frac{1}{C_m} \right) \delta Q_m^2 + \frac{\phi_m^2}{2L_m} + \frac{\delta Q \delta Q_m}{\bar{C}_c}, \end{aligned} \quad (13)$$

where $\delta Q_m, \phi_m$ are charge and magnetic flux variables of the virtual mechanical branch. The first two terms of Eq. (13) are the charging energies of the two capacitors, and the third term is the virtual magnetic field energy of the equivalent mechanical inductor. The fourth term, which is essential for the transducer, is a bilinear coupling between the mechanical oscillation and the charge on the coupling capacitor.

We can check the ansatz (10) and find expressions for the equivalent circuit parameters in terms of EM quantities by comparing Eqs. (11) and (13) term by term (the terms in the two expressions are ordered in the same way). We first compare the last (coupling) terms. These become identical if we make the identification

$$\delta Q_m = \bar{C}_c G \delta x, \quad (14)$$

that is, the charge variable of the virtual mechanical arm is proportional to the mechanical displacement. Given the above correspondence, we expect a similar relationship among the canonical conjugates, $\phi_m \propto p$. Taking the time derivative we indeed find

$$p = m \delta \dot{x} = \frac{m}{\bar{C}_c G} \delta \dot{Q}_m = \frac{m}{\bar{C}_c G} I_m = \frac{m}{\bar{C}_c G L_m} \phi_m, \quad (15)$$

using Eq. (14), $\phi_m = L_m \delta \dot{Q}_m$, and $I_m \equiv \delta \dot{Q}_m$. Equating the inductive energy term of Eq. (13) with the kinetic of Eq. (11) and substituting using Eq. (15), we find an expression for L_m

$$\frac{p^2}{2m} = \frac{\phi_m^2}{2L_m} \Leftrightarrow L_m = \frac{m}{\bar{C}_c^2 G^2}. \quad (16)$$

Substituting L_m into Eq. (15) we then find

$$\phi_m = \frac{1}{\bar{C}_c G} p. \quad (17)$$

Taken together, Eqs. (14,17) show that the dynamical variables of the equivalent circuit $\{\delta Q_m, \phi_m\}$ are related to the original coordinates $\{\delta x, p\}$ by a simple canonical scaling transformation.

Finally, we determine the equivalent mechanical resistance R_m , which is most easily done by comparing equations of motion (where damping can be incorporated straightforwardly). Equating the viscous dissipation rate in Eq. (1) with $\dot{\phi}_m = -(R_m/L_m)\phi_m + \dots$ we get

$$R_m = \gamma_{m,0} L_m = \frac{m \gamma_{m,0}}{\bar{C}_c^2 G^2}, \quad (18)$$

using the expression in Eq. (16) for L_m . Similarly, by comparing Eq. (1) with $\dot{\phi}_m = 2V_m + \dots$, we find that the fluctuating mechanical force F maps to a voltage

$$2V_m \equiv \frac{F}{G\bar{C}_c}, \quad (19)$$

where the factor of two has been included to conform with the electrical input-output formalism to be presented in Section V, cf. Eq. (44). By considering the spectrum of the noise (2,3) it is found that V_m , as given by Eq. (19), is exactly the Johnson noise of a resistor with resistance R_m .

B. Effective mechanical resonance frequencies

There is a subtlety related to the effective resonance frequency of the mechanical mode, which depends on how the time-scale of the mechanical mode δQ_m compares to that of the electrical mode δQ . Two different limits can be understood from Fig. 2b and Eq. (13), namely fixed voltage versus fixed charge dynamics. Fixed voltage across the terminals of Fig. 2b corresponds to the situation where the voltage bias in the circuit acts much faster than the mechanical modulation, i.e., supplying and absorbing charge instantaneously so as to maintain a fixed voltage. The voltage across the mechanical arm will in this case be independent of the capacitor arm; therefore we may read off the *fixed voltage* mechanical resonance frequency as the resonance frequency of the mechanical branch of Fig. 2b:

$$\omega_{m,V}^2 = \frac{1}{L_m C_m}, \quad (20)$$

sometimes referred to as the mechanical series resonance [48]. For a given applied voltage across the coupling capacitor, the maximal mechanical response occurs at $\omega_{m,V}$. If, on the other hand, the time-scale of mechanical modulation is much faster than that of δQ (thus preventing the voltage bias from reacting), we may effectively set $\delta Q \rightarrow 0$. The *fixed charge* mechanical resonance frequency will then be the resonance frequency of the entire loop in Fig. 2b in which case the capacitances \bar{C}_c, C_m are added in series

$$\omega_{m,Q}^2 = \frac{1}{L_m} \left(\frac{1}{\bar{C}_c} + \frac{1}{C_m} \right). \text{ [DC bias]} \quad (21)$$

This is sometimes referred to as the mechanical parallel resonance [48]. This is also the relation obtained by equating the second terms in Eqs. (11,13). For a given current running into the (physical) coupling capacitor $C_c(x)$, the maximal mechanical response occurs at $\omega_{m,Q}$. By comparing Eqs. (20) and (21) we see that the two limiting mechanical frequencies are related by

$$\omega_{m,Q}^2 - \omega_{m,V}^2 = \frac{1}{L_m \bar{C}_c} = \frac{\bar{C}_c G^2}{m}, \text{ [DC bias]} \quad (22)$$

from which we conclude that $\omega_{m,Q} \geq \omega_{m,V}$. The mechanical oscillator thus has a different resonance frequency depending on the circuit to which it is coupled (i.e., including circuit elements not shown in Fig. 2b). For instance, if the bias voltage is applied via a low-pass filter with cut-off frequency below the mechanical frequency (as in Ref. [34]) this entails fixed charge conditions. From the expression for $\omega_{m,Q}^2$ (12) and the relation in Eq. (22), we can find an expression for $\omega_{m,V}$ in terms of the known physical quantities,

$$\omega_{m,V}^2 = \omega_{m,0}^2 - \frac{\langle \bar{Q}_c^2(t) \rangle}{2m \bar{C}_c^2} \frac{d^2 C_c}{dx^2} \Big|_{x=\bar{x}}. \quad (23)$$

Using Eqs. (16,20) we can then express the mechanical capacitance through quantities which can be calculated from first principles

$$C_m = \frac{\bar{C}_c^2 G^2}{\omega_{m,V}^2 m}. \quad (24)$$

IV. ELECTROMECHANICAL EQUIVALENT CIRCUIT FOR AC DRIVE

Above we have given an intuitive derivation of the equivalent circuit in the case of a DC-biased capacitor. This allows us to describe how electrical signals are converted into mechanical motion at the same frequency. The typical purpose of a transducer is, however, to convert signals from one frequency Ω to another $\omega_d \pm \Omega$ by harmonically driving the system with a frequency ω_d . In the following we shall develop an equivalent circuit formalism to describe this situation in the regime where ω_d is much larger than the mechanical resonance frequency. This can, e.g., correspond to a mechanical oscillator in the MHz regime driven by a voltage in the GHz range.

When the capacitor is driven by an alternating voltage the charge on the capacitor will take the form

$$Q(t) = \bar{Q}_c(t) + \delta Q(t) = \bar{Q}_{c,0} (e^{-i\omega_d t} + e^{i\omega_d t}) + \delta Q(t), \quad (25)$$

c.f. Eq. (7), where we for simplicity take the amplitude $\bar{Q}_{c,0}$ to be real. Similar to above, this amplitude should be found by self-consistently solving for the equilibrium configuration of the electrical and mechanical system, and $\delta Q(t)$

then represents the fluctuations around this value. It will be convenient to work in the Fourier domain following the standard linear response approach. Exploiting that all charges, currents, and voltages are real valued, we introduce the Fourier transform as an integral over positive frequencies so that, e.g., the voltage fluctuations are denoted by

$$\delta V(t) = \int_0^\infty \frac{d\omega}{\sqrt{2\pi}} [V(\omega)e^{-i\omega t} + V^*(\omega)e^{i\omega t}] \quad (26)$$

with similar expressions for the charge δQ and current δI fluctuations as well as the position δx and momentum p fluctuations. To proceed, it is convenient not to deal with the specifics of the rest of the circuit and we therefore replace it with its Thévenin equivalent diagram [59] as shown in Fig. 3a, i.e., it is represented by an ideal voltage source δV and the input impedance Z . If we now consider the contribution to Kirchoff's law coming from the coupled EM system we have

$$\delta V(t) = \dots + \frac{Q(t)}{C_c(x)} - \frac{\bar{Q}_{c,0} (e^{-i\omega_d t} + e^{i\omega_d t})}{\bar{C}_c} \quad (27)$$

$$\approx \dots + \frac{\delta Q(t)}{\bar{C}_c} + G\delta x(t) (e^{-i\omega_d t} + e^{i\omega_d t}), \quad (28)$$

where the ellipsis represents terms arising from the rest of the circuit. In the last line we have expanded to lowest order in the fluctuations and introduced the coupling constant G as defined in Eq. (9).

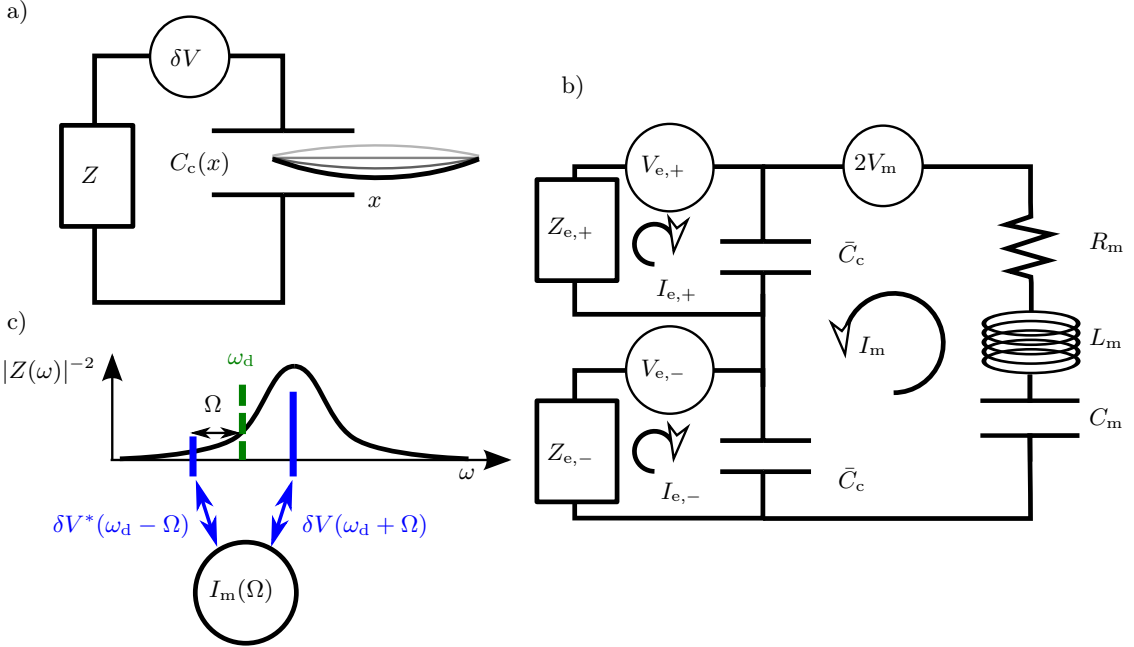


Figure 3. a) Thévenin equivalent circuit considered for the AC-driven system. An ideal voltage source $\delta V(\omega)$ in series with an impedance $Z(\omega)$ drives the coupled membrane capacitor system. b) EM equivalent circuit. The mechanical motion is replaced by the central loop current $I_m(\Omega)$. Through capacitors of capacitance \bar{C}_c , the mechanical current is connected to loop currents $I_{e,+}$ and $I_{e,-}$ representing the upper and lower sidebands of the electrical current, which are driven by voltage sources $V_{e,+}(\Omega) = \delta V(\omega_d + \Omega)$ and $V_{e,-}(\Omega) = \delta V^*(\omega_d - \Omega)$. c) Sketch of the spectral mapping between the electrical and mechanical frequency scales. The electrical spectrum is folded around the carrier frequency ω_d (with a gain profile determined by $Z(\omega)$) such that the upper and lower sidebands at $\omega_d \pm \Omega$ are mapped into a single mechanical frequency Ω .

We will now assume that the mechanical component is the slowest frequency scale in the problem so that we can neglect the mechanical response, $\delta x(\omega) \approx 0$, at high frequencies $\omega > \omega_d$. This amounts to the assumption that the mechanical resonance frequency is small compared to ω_d . With this assumption, the mechanical frequency component $\delta x(\Omega) \propto I_m(\Omega)$ will couple to two frequency components of the electrical circuit located at the upper and lower sidebands of the drive, $\delta V(\omega_d + \Omega)$ and $\delta V^*(\omega_d - \Omega)$, as illustrated in Fig. 3c. We thus arrive at

$$\delta V(\omega_d + \Omega) = Z(\omega_d + \Omega)\delta I(\omega_d + \Omega) + \frac{\delta Q(\omega_d + \Omega)}{\bar{C}_c} - G\delta x(\Omega) \quad (29)$$

$$\delta V^*(\omega_d - \Omega) = Z^*(\omega_d - \Omega)\delta I^*(\omega_d - \Omega) + \frac{\delta Q^*(\omega_d - \Omega)}{\bar{C}_c} - G\delta x(\Omega) \quad (30)$$

Here $\Omega > 0$ denotes the small frequency of the excursion of the mechanical oscillator, which the electrical circuits sees as a frequency relative to the band center ω_d . Eqs. (29,30) determine the circuit response above and below the center frequency, respectively, at the 'lab frame' frequency $\omega = \omega_d \pm \Omega$. From this expression the principle of the transducer is apparent: the oscillating drive connects different frequency components of the mechanical and electrical circuit. Eqs. (29,30) also show that electrical frequency components are mapped into the mechanical mode in a non-invertible, 2-to-1 manner. This characteristic is the key to establishing a relatively simple equivalent circuit for the AC case below. As we will see, *we may consider the upper and lower electrical sidebands, (29) and (30), to be distinct degrees of freedom coupling to the mechanical mode.*

We now turn to the mechanical oscillator. By combining the interaction Hamiltonian (8) with Eq. (1) we may derive the equation of motion for the mechanical momentum

$$\dot{p} = -m\omega_{m,V}^2 \delta x - \gamma_{m,0} p + F(t) - G(e^{-i\omega_d t} + e^{i\omega_d t}) \delta Q - 2G^2 \bar{C}_c \delta x. \quad (31)$$

In the above expression we have averaged over oscillations occurring with a frequency $2\omega_d$ in accordance with the assumption that the mechanical response only happens on a slower time scale. Compared to the DC-biased case, where $\omega_{m,Q}$ and $\omega_{m,V}$ are related by Eq. (22), this averaging in the AC case gives a factor of two appearing on the right-hand side of Eq. (22) and hence in the last term of Eq. (31). For later convenience we have again introduced $\omega_{m,V}$ from Eq. (23) which we will again identify as the resonance frequency at fixed voltage.

To find the equivalent circuit representation, we convert Eq. (31) to Fourier space and introduce the electrical analogs of the mechanical parameters as defined in Eqs. (14)–(16), (18), (19) and (24). We thereby find

$$2V_m(\Omega) = -i\Omega L_m I_m(\Omega) + R_m I_m(\Omega) + \frac{\delta Q_m(\Omega)}{C_m} + \frac{2\delta Q_m(\Omega) + \delta Q(\omega_d + \Omega) + \delta Q^*(\omega_d - \Omega)}{\bar{C}_c}. \quad (32)$$

This expression for the momentum (represented by I_m) resembles Kirchoff's voltage law, except for the mixing of different frequency components and the appearance of the complex conjugate. To remove these differences, we define new voltages and charges for the upper and lower sidebands of the drive

$$V_{e,+}(\Omega) = \delta V(\omega_d + \Omega) \quad V_{e,-}(\Omega) = \delta V^*(\omega_d - \Omega) \quad (33)$$

$$Q_{e,+}(\Omega) = \delta Q(\omega_d + \Omega) \quad Q_{e,-}(\Omega) = \delta Q^*(\omega_d - \Omega). \quad (34)$$

For the current we wish to retain the standard relation $I_{e,\pm}(\Omega) = -i\Omega Q_{e,\pm}(\Omega)$. We achieve this with the choice

$$I_{e,+}(\Omega) = \frac{\Omega}{\omega_d + \Omega} I(\omega_d + \Omega) \quad I_{e,-}(\Omega) = -\frac{\Omega}{\omega_d - \Omega} I^*(\omega_d - \Omega), \quad (35)$$

where the minus sign in the last expression is a consequence of the complex conjugation. Correspondingly we have the upper and lower sideband impedances

$$Z_{e,+}(\Omega) = \frac{\omega_d + \Omega}{\Omega} Z(\omega_d + \Omega) \quad Z_{e,-}(\Omega) = -\frac{\omega_d - \Omega}{\Omega} Z^*(\omega_d - \Omega). \quad (36)$$

Here the combination of the negative sign and the complex conjugation in $Z_{e,-}$ means that reactances retain their sign whereas resistances have their sign flipped. This reflects the instability associated with the coupling to the lower sideband, which yields parametric amplification, manifesting the active character of the circuit (the drive field being the source of energy). Furthermore, the prefactor in Eq. (36) means that capacitors keep their usual expression for the impedance $1/(-i\Omega C)$ whereas inductances and resistances are scaled up to reflect that it is harder to induce a given charge amplitude at a higher frequency. Combining these definitions with the equations of motion in Eqs. (29), (30), and (32), we finally achieve

$$2V_m(\Omega) = \left[-i\Omega L_m + R_m + \frac{1}{-i\Omega C_m} \right] I_m(\Omega) + \frac{2I_m(\Omega) + I_{e,+}(\Omega) + I_{e,-}(\Omega)}{-i\Omega \bar{C}_c} \quad (37)$$

$$V_{e,\pm}(\Omega) = Z_{e,\pm}(\Omega) I_{e,\pm}(\Omega) + \frac{I_{e,\pm}(\Omega) + I_m(\Omega)}{-i\Omega \bar{C}_c} \quad (38)$$

These equations of motion have a straightforward interpretation in terms of the equivalent circuit diagram in Fig. 3b. Here the mechanical system is represented by the loop current I_m in the central loop, whereas the outer loops represent the upper and lower sidebands of the electrical system. We remark that the divergent behavior of L_m , R_m , V_m , and $1/C_m$ (16,18,19,24) for vanishing EM coupling, $G \rightarrow 0$, serves to decouple the mechanical loop from the rest of the circuit as expected.

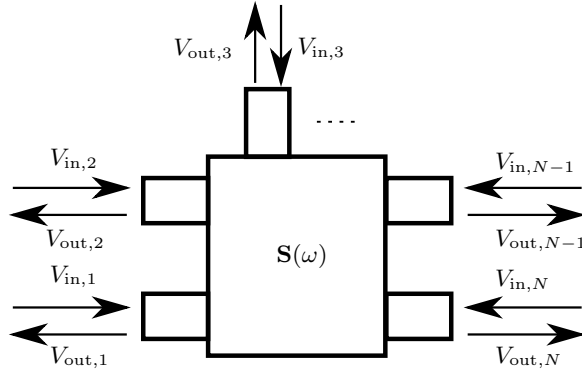


Figure 4. Illustration of the scattering matrix $\mathbf{S}(\omega)$.

From the circuit, it is immediately apparent that $\omega_{m,V} = 1/\sqrt{L_m C_m}$ is the mechanical resonance frequency in the limit where the capacitor is connected to an ideal voltage source $Z_{e,+} = Z_{e,-} = 0$, so that the outer arms are replaced by short circuits bypassing the capacitors of capacitance \bar{C}_c . On the other hand, for fixed charge $Z_{e,+}, Z_{e,-} \rightarrow \infty$, the mechanical resonance frequency $\omega_{m,Q}$ is shifted from $\omega_{m,V}$ by twice the amount given in Eq. (22) since \bar{C}_c appears for both sidebands. This completes the derivation of the equivalent circuit. With the results developed here the analysis of the coupled EM system can now be reduced to finding voltages and current of linear circuits. This gives a direct description of how voltage fluctuations are transduced to the mechanical system and vice versa.

As an example, we consider a serial RLC with resonance frequency $\bar{\omega}_{LC} = 1/\sqrt{L\bar{C}_c} \sim 1\text{GHz}$ capacitively coupled to the position of a mechanical element resonating in the regime $\omega_{m,Q} \sim 1\text{MHz}$ by means of a drive tone of frequency $\omega_d \sim \bar{\omega}_{LC} \gg \omega_{m,Q}$. In this case the Thévenin impedance of the electrical resonance Z appearing in Fig. 3a is $Z(\omega) = -i\omega L + R$, so that the equivalent impedances of the upper and lower electrical sidebands are, from Eqs. (36),

$$Z_{e,+}(\Omega) = -i \frac{(\omega_d + \Omega)^2}{\Omega} L + \frac{\omega_d + \Omega}{\Omega} R \quad (39)$$

$$Z_{e,-}(\Omega) = -i \frac{(\omega_d - \Omega)^2}{\Omega} L - \frac{\omega_d - \Omega}{\Omega} R. \quad (40)$$

As mentioned above, the negative resistance of the lower sideband gives rise to amplification effects reflecting the instability of the lower sideband.

V. ELECTRICAL INPUT-OUTPUT FORMALISM

In the preceding sections we have derived an equivalent impedance description of EM systems. We will now extend this to describe how signals and noise enter and exit the system via its various ports, which is essential to the analysis of transducers. Our analysis generalizes the network analysis employed in the characterization of passive, purely electrical radio-frequency and microwave circuits [60]. Such electrical input-output formalism amounts to supplementing Kirchhoff's circuit laws with equations relating the input and output signals of (virtual) transmission lines to the currents in the circuit. Solving these equations in the context of a linear N-port circuit, see Fig. 4, the outgoing signals can be related to the incoming ones by the classical scattering matrix

$$\vec{V}_{\text{out}}(\Omega) = \mathbf{S}(\Omega) \vec{V}_{\text{in}}(\Omega), \quad (41)$$

where $\vec{V}_{\text{in/out}}(\Omega)$ is a vector containing the complex amplitudes of the incoming and outgoing traveling waves.

To derive a scattering relation of the form of Eq. (41) for our system, we shall use the equivalent circuit description derived above. Physically, the input and output ports of the equivalent circuit are transmission lines, resistive elements, and mechanical dissipation. The mechanical force was converted into its Johnson voltage equivalent in Eq. (19) and this suffices for DC-biased transducers. However, for the AC-driven EM circuit, frequency interconversion must be accounted for. To accommodate this in the electrical input-output formalism, the vectors of inputs and outputs $\vec{V}_{\text{in/out}}(\Omega)$ is generalized to ($p \in \{\text{in}, \text{out}\}$)

$$\vec{V}_p(\Omega) = (V_{p,m}(\Omega), V_{p,1}(\omega_{d,1} + \Omega), V_{p,1}^*(\omega_{d,1} - \Omega), V_{p,2}(\omega_{d,2} + \Omega), V_{p,2}^*(\omega_{d,2} - \Omega), \dots)^T, \quad (42)$$

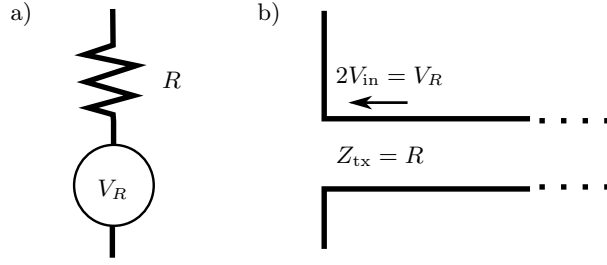


Figure 5. Mapping between a) a resistor R with Johnson voltage noise V_R and b) a semi-infinite lossless transmission line with characteristic impedance $Z_{\text{tx}} = R$ and incoming signal $2V_{\text{in}} = V_R$.

where $V_{\text{in},m} \equiv V_m$ and we allow for the possibility of multiple drive fields $\omega_{d,i}$ (as will be relevant when adding, e.g., an optical subsystem). Hence, Eq. (41) together with Eq. (42) captures both the frequency interconversion between subsystems as well as the mixing of sideband signals.

To link the external input and output fields in $\vec{V}_{\text{in/out}}(\Omega)$ to the internal currents and voltages in the impedance formalism, we recall how the presence of a port in the circuit modifies Kirchhoff's equations. To this end, we observe that the voltage V_i across and the net (physical) current amplitude I_i into the i 'th terminal can be expressed in terms of the travelling wave amplitudes at the terminal as

$$\begin{aligned} V_i &= V_{\text{in},i} + V_{\text{out},i} \\ I_i &= \frac{1}{Z_{\text{tx},i}} [V_{\text{in},i} - V_{\text{out},i}]. \end{aligned} \quad (43)$$

From Eqs. (43) we can derive the equivalent of a fluctuation-dissipation relation for each port [46],

$$V_i = -Z_{\text{tx},i} I_i + 2V_{\text{in},i}. \quad (44)$$

Eq. (44) is the key to extending Kirchhoff's laws to an open system setting. Specifically, for Kirchhoff's voltage law for any loop including one of the ports, it tells us that the port introduces dissipation corresponding to the real-valued resistance $R = Z_{\text{tx},i}$, as well as a source term $2V_{\text{in},i}$. Conversely, as pointed out by Nyquist [61], this implies that any resistive element R in the circuit can be mapped to an equivalent semi-infinite transmission line of characteristic impedance $Z_{\text{tx},j} = R$, while the Johnson noise of the resistor is included by specifying a thermal mixed state for the corresponding source term $V_{\text{in},j}$; this mapping is illustrated in Fig. 5. In this way, the resulting open circuit formalism puts noise and signal inputs on equal footing. From Eq. (43) we can also derive the input-output relations for the ports,

$$V_{\text{out},i} = -Z_{\text{tx},i} I_i + V_{\text{in},i}, \quad (45)$$

that allow us to determine the itinerant outgoing voltages.

With the above in place, we may, for an arbitrary N-port passive linear circuit, use Kirchhoff's circuit laws supplemented with Eqs. (44) and (45) to derive the scattering matrix $\mathbf{S}(\omega)$. In practice this can, e.g., be done by applying standard impedance rules to the equivalent circuit diagram under consideration as will be demonstrated below. Once the scattering matrix $\mathbf{S}(\Omega)$ (41) has been obtained, we have a full characterization of the dynamics of the transducer. When the initial state of all the involved reservoirs is specified, the scattering matrix can therefore be used to evaluate the performance of the transducer for whichever application one is interested in [62].

Before quantizing the theory and generalizing the formalism to accommodate optomechanical interfaces, we illustrate the usefulness of the equivalent circuit for determining the scattering matrix for an AC-driven EM interface. We treat the example of a serial RLC circuit with ohmic resistance R_{LC} coupled to a transmission line (of characteristic impedance Z_{tx}) and capacitively coupled to a mechanical mode (see Fig. 6a). Hence, the electrical subsystem is characterized by the Thévenin impedance

$$Z(\omega) = -i\omega L + R_{\text{LC}} + Z_{\text{tx}}, \quad (46)$$

where L is the inductance in the electrical circuit and, for later convenience, we define $\bar{\omega}_{\text{LC}} \equiv (L\bar{C}_c)^{-1/2}$. Since the current is the same through the circuit elements R_{LC} and Z_{tx} , the fraction of the power dissipated in the circuit that goes into the transmission line is

$$\eta_{\text{el}} \equiv Z_{\text{tx}} / (R_{\text{LC}} + Z_{\text{tx}}), \quad (47)$$

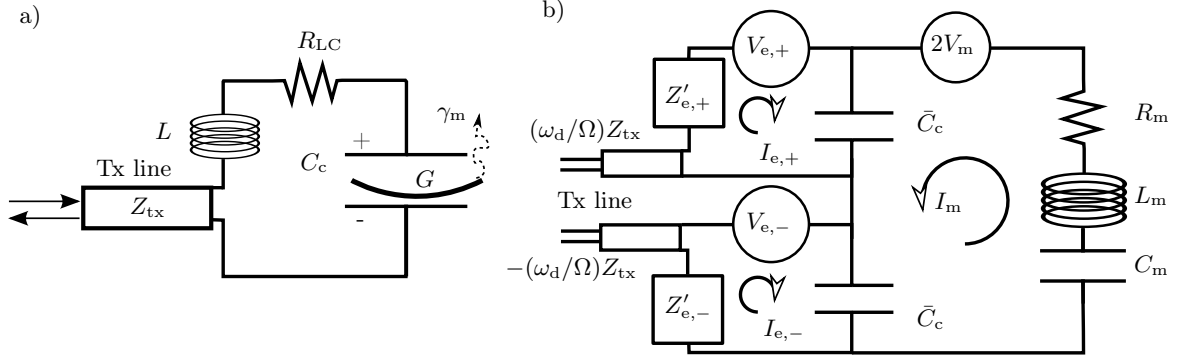


Figure 6. a) RLC circuit (ohmic resistance R_{LC}) coupled to a single transmission line of characteristic impedance Z_{tx} and, at the same time, capacitively coupled to a mechanical mode (intrinsic damping rate γ_m) by means of an AC-drive of frequency ω_d (not shown) resulting in an EM coupling strength G . b) EM equivalent circuit for the system depicted in a). The transmission line impedance Z_{tx} loads the upper/lower sideband loop by $\sim \pm(\omega_d/\Omega)Z_{tx}$ [Eqs. (39,40), for $\Omega \ll \omega_d$] (the inductor and the ohmic loss resistor are represented by $Z'_{e,\pm}$). In the quantum limit, the interaction of the electrical sideband fields $V_{e,\pm}$ with the mechanical system can lead to squeezing of the outgoing transmission line signal.

sometimes referred to as the electrical coupling efficiency. Each of the decay channels induce a (Johnson) voltage source contributing to the Thévenin voltage (see Fig. 3a)

$$\delta V(\omega) = 2V_{e,\text{in}}^{(LC)}(\omega) + 2V_{e,\text{in}}^{(\text{tx})}(\omega), \quad (48)$$

as follows from Eq. (44). The electrical output fields are given by the input-output relations (45). For the serial RLC considered here (46), whose conventional circuit diagram only has a single loop current, the electrical transmission line output is given by

$$V_{e,\text{out}}^{(\text{tx})}(\omega_d + \Omega) = -\frac{\omega_d + \Omega}{\Omega} Z_{tx} I_{e,+}(\Omega) + V_{e,\text{in}}^{(\text{tx})}(\omega_d + \Omega) \quad (49)$$

$$V_{e,\text{out}}^{(\text{tx})*}(\omega_d - \Omega) = \frac{\omega_d - \Omega}{\Omega} Z_{tx} I_{e,-}(\Omega) + V_{e,\text{in}}^{(\text{tx})*}(\omega_d - \Omega), \quad (50)$$

expressed in terms of the upper and lower sideband electrical loop currents $I_{e,\pm}(\Omega)$ by means of Eqs. (35).

To use Eqs. (49,50) to establish the scattering matrix (41), we need to determine the electrical loop currents $I_{e,\pm}$. Rather than solving Kirchhoff's equations (37,38) algebraically, the transfer coefficients can be obtained by applying simple impedance rules to the corresponding equivalent circuit, Fig. 6b. To this end, it is convenient to introduce the effective impedance of the central (mechanical) loop,

$$Z_{m,\text{eff}}(\Omega) = Z_m(\Omega) + \Delta Z(\Omega), \quad (51)$$

where the bare mechanical impedance Z_m (10) is loaded by the electrical sideband loops,

$$\Delta Z(\Omega) = \sum_{s=\pm} [-i\Omega\bar{C}_c + 1/Z_{e,s}(\Omega)]^{-1} = \sum_{s=\pm} \frac{1 + \mathcal{Q}_{e,s}(\Omega)}{-i\Omega\bar{C}_c}, \quad (52)$$

where in the final expression we have expressed the load from sideband s as a sum of the impedance of its coupling capacitor and a contribution proportional to its susceptibility function (in the rotating frame of the AC drive),

$$\mathcal{Q}_{e,\pm}(\Omega) \equiv -\frac{1/(-i\Omega\bar{C}_c)}{Z_{e,\pm}(\Omega) + 1/(-i\Omega\bar{C}_c)}. \quad (53)$$

The contributions $s = \pm$ to Eq. (52) are simply the Thévenin impedances of the respective sideband loops *including* the coupling capacitor. For the present example of an AC-driven serial RLC circuit, the electrical susceptibilities for the two sidebands have the standard form for the response of a resonant circuit,

$$\mathcal{Q}_{e,\pm}(\Omega) = -\frac{\bar{\omega}_{LC}^2}{\bar{\omega}_{LC}^2 - (\omega_d \pm \Omega)^2 \mp i(\omega_d \pm \Omega)R_{\text{tot}}/L}, \quad (54)$$

where $R_{\text{tot}} \equiv R_{\text{LC}} + Z_{\text{tx}}$.

Using the rule of voltage division across serially connected elements, the electrical voltage sources representing the incoming transmission line signal $V_{e,\pm}$ are seen to induce a voltage $-V_{e,\pm}(\Omega)(-i\Omega\bar{C}_c)^{-1}/[Z_{e,\pm}(\Omega) + (-i\Omega\bar{C}_c)^{-1}]$ across their respective (virtual) coupling capacitors (of capacitance \bar{C}_c), adding to the voltage $2V_m(\Omega)$ in the mechanical loop. The mechanical loop current response I_m to this net voltage follows by multiplication by the loaded mechanical admittance $1/Z_{m,\text{eff}}$ (51). Having determined I_m , it can be considered a current source from the point of view of the electrical sideband loops, and in terms of this the electrical sideband currents are simply $I_{e,\pm}(\Omega) = [V_{e,\pm}(\Omega) - I_m(-i\Omega\bar{C}_c)^{-1}]/[Z_{e,\pm}(\Omega) + (-i\Omega\bar{C}_c)^{-1}]$. Expressing these observations in terms of the functions $\mathcal{Q}_{e,\pm}(\Omega)$ (53) and putting them together, the sideband loop currents are found to be,

$$I_{e,\pm}(\Omega) = \mathcal{Q}_{e,\pm}(\Omega) \left[\frac{\mathcal{Q}_{e,\pm}(\Omega)}{Z_{m,\text{eff}}(\Omega)} + i\Omega\bar{C}_c \right] V_{e,\pm}(\Omega) + \frac{\mathcal{Q}_{e,\pm}(\Omega)\mathcal{Q}_{e,\mp}(\Omega)}{Z_{m,\text{eff}}(\Omega)} V_{e,\mp}(\Omega) + \frac{\mathcal{Q}_{e,\pm}(\Omega)}{Z_{m,\text{eff}}(\Omega)} 2V_m(\Omega). \quad (55)$$

Using Eqs. (33,48-50) we arrive at the scattering relation in terms of the itinerant fields (considering the overcoupled limit, $R_{\text{LC}} \rightarrow 0$, for simplicity),

$$\begin{pmatrix} V_{e,\text{out}}^{(\text{tx})}(\omega_d + \Omega) \\ V_{e,\text{out}}^{(\text{tx})*}(\omega_d - \Omega) \end{pmatrix} = \begin{pmatrix} D(\Omega) & O(\Omega) \\ O^*(-\Omega) & D^*(-\Omega) \end{pmatrix} \begin{pmatrix} V_{e,\text{in}}^{(\text{tx})}(\omega_d + \Omega) \\ V_{e,\text{in}}^{(\text{tx})*}(\omega_d - \Omega) \end{pmatrix} + \begin{pmatrix} M(\Omega) \\ M^*(-\Omega) \end{pmatrix} V_m(\Omega), \quad (56)$$

where the coefficients are given by

$$D(\Omega) \equiv 1 - 2i(\omega_d + \Omega)\bar{C}_c Z_{\text{tx}} \mathcal{Q}_{e,+}(\Omega) - 2\frac{\omega_d + \Omega}{\Omega} Z_{\text{tx}} \frac{\mathcal{Q}_{e,+}^2(\Omega)}{Z_{m,\text{eff}}(\Omega)}, \quad (57)$$

$$O(\Omega) \equiv -2\frac{\omega_d + \Omega}{\Omega} Z_{\text{tx}} \frac{\mathcal{Q}_{e,+}(\Omega)\mathcal{Q}_{e,-}(\Omega)}{Z_{m,\text{eff}}(\Omega)}, \quad (58)$$

$$M(\Omega) \equiv -2\frac{\omega_d + \Omega}{\Omega} Z_{\text{tx}} \frac{\mathcal{Q}_{e,+}(\Omega)}{Z_{m,\text{eff}}(\Omega)}, \quad (59)$$

having made use of the properties $\mathcal{Q}_{e,-}^*(\Omega) = \mathcal{Q}_{e,+}(-\Omega)$ [Eqs. (36,53)] and $Z_{m,\text{eff}}^*(\Omega) = Z_{m,\text{eff}}(-\Omega)$. The scattering relation (56) fully characterizes the linearized interaction of the system and thus contains, e.g., all of the physical effects familiar from the analogous setup in linearized optomechanics: e.g., dynamical back-action on the mechanical mode (“optical spring effect”) [3], Optomechanically Induced Transparency [63], and classical noise squashing [64].

VI. QUANTIZATION OF THE EQUIVALENT CIRCUIT

We now turn to the quantization of our circuit theory. Because our system is described by a bilinear Hamiltonian, the Heisenberg-Langevin equations are algebraically equivalent to their classical counterpart. Hence, the scattering matrix is identical in the quantum and classical cases. We therefore do not need to consider the internal degrees of freedom of the circuit (i.e., its quasi-localized normal modes) and it suffices to expand the itinerant voltage amplitudes (42), including noise sources [with the representation in Fig. 5], using quantized ingoing and outgoing fields. Writing this in the frequency domain, we have [65]

$$\hat{V}_{p,i}(t) = \int_0^\infty \frac{d\omega}{\sqrt{2\pi}} \sqrt{\frac{\hbar\omega Z_{\text{tx},i}}{2}} \left[\hat{b}_{p,i}(\omega) e^{-i\omega t} + \text{H.C.} \right], \quad (60)$$

where the annihilation operators $\hat{b}_{p,i}(\omega)$, $p \in \{\text{in}, \text{out}\}$ obey the commutation relations

$$[\hat{b}_{p,i}(\omega), \hat{b}_{p,j}^\dagger(\omega')] = \delta(\omega - \omega') \delta_{i,j}, \quad (61)$$

with all other commutators being zero. Eqs. (60,61) specify the correct ohmic noise operator that enters the quantum version of Eq. (44), i.e., within the Markov approximation of a memoryless reservoir [50]. This expansion has the same form as the Fourier transform introduced in Eq. (26), and hence we can immediately identify the corresponding voltage operators which replace their classical counterparts

$$\begin{aligned} V_{p,i}(\omega) &\rightarrow \hat{V}_{p,i}(\omega) = \sqrt{\frac{\hbar\omega Z_{\text{tx},i}}{2}} \hat{b}_{p,i}(\omega) \\ V_{p,i}^*(\omega) &\rightarrow \hat{V}_{p,i}^\dagger(\omega) = \sqrt{\frac{\hbar\omega Z_{\text{tx},i}}{2}} \hat{b}_{p,i}^\dagger(\omega), \end{aligned} \quad (62)$$

where again $p \in \{\text{in}, \text{out}\}$. From these expressions we can then find the corresponding upper and lower sideband operators entering the equivalent circuit using Eq. (33).

To characterize the noise we will assume that all reservoirs are in their thermal state as specified by the expectation values ($\omega, \omega' > 0$)

$$\begin{aligned}\langle \hat{V}_{\text{in},i}^\dagger(\omega) \hat{V}_{\text{in},j}(\omega') \rangle &= \frac{\hbar\omega Z_{\text{tx},i}}{2} n_i(\omega) \delta(\omega - \omega') \delta_{i,j} \\ \langle \hat{V}_{\text{in},i}(\omega) \hat{V}_{\text{in},j}^\dagger(\omega') \rangle &= \frac{\hbar\omega Z_{\text{tx},i}}{2} [n_i(\omega) + 1] \delta(\omega - \omega') \delta_{i,j}\end{aligned}\quad (63)$$

and $\langle \hat{V}_{\text{in},i}(\omega) \hat{V}_{\text{in},j}(\omega') \rangle = 0 = \langle \hat{V}_{\text{in},i}^\dagger(\omega) \hat{V}_{\text{in},j}^\dagger(\omega') \rangle$, where the thermal flux per unit bandwidth is given by the Bose-Einstein distribution (4). Note that Eqs. (63) are completely equivalent to those pertaining to quantum Brownian motion (3) considered previously. Due to the linearly rising term $\propto \omega$ in the second line of Eqs. (63), a cutoff is required to avoid divergences when integrating over all spectral components [50]; in this article, however, we shall only consider finite frequency ranges. The thermal expectation values of the mechanical Johnson voltage $V_m(\Omega)$ (19) take the same form as Eqs. (63) with the replacements $Z_{\text{tx},i} \rightarrow R_m, T_i \rightarrow T_m$ [51]. With these replacements the scattering matrix derived from the equivalent circuit yields a complete characterization of the performance of the transducer also in the quantum regime.

We demonstrate the quantization procedure by continuing the above example of an AC-driven EM interface [Fig. 6]. The scattering matrix (56) for the voltage amplitudes is unchanged under quantization. However, in the quantum domain it is more customary to work with the bosonic operators (61), whose scattering matrix differs from that of the voltage amplitudes due to the different zero-point amplitudes (62) of the various itinerant fields. Hence, from Eqs. (56,62) we have

$$\begin{pmatrix} \hat{b}_{\text{out}}^{(\text{tx})}(\omega_d + \Omega) \\ \hat{b}_{\text{out}}^{(\text{tx})\dagger}(\omega_d - \Omega) \end{pmatrix} = \begin{pmatrix} D(\Omega) & O'(\Omega) \\ O'^*(-\Omega) & D^*(-\Omega) \end{pmatrix} \begin{pmatrix} \hat{b}_{\text{in}}^{(\text{tx})}(\omega_d + \Omega) \\ \hat{b}_{\text{in}}^{(\text{tx})\dagger}(\omega_d - \Omega) \end{pmatrix} + \begin{pmatrix} M'(\Omega) \\ M'^*(-\Omega) \end{pmatrix} \hat{c}_{\text{in}}(\Omega), \quad (64)$$

where $\hat{c}_{\text{in}}(\Omega)$ is the mechanical noise input field operator analogous to $\hat{b}_{\text{in}}^{(\text{tx})}$ [using the representation of Fig. 5], and we have defined the modified transfer functions [cf. Eqs. (58,59)]

$$O'(\Omega) \equiv \sqrt{\frac{\omega_d - \Omega}{\omega_d + \Omega}} O(\Omega), \quad (65)$$

$$M'(\Omega) \equiv \sqrt{\frac{|\Omega|}{\omega_d + \Omega} \frac{R_m}{Z_{\text{tx}}}} M(\Omega). \quad (66)$$

As an example, the quantized theory allows us to discuss the ponderomotive squeezing of the outgoing electromagnetic field [15, 66, 67] that can result for our example circuit [Fig. 6]. This can be understood as two-mode squeezing [68] of the upper and lower sidebands. Hence, using Eq. (64) along with Eqs. (4,63), we evaluate the spectrum of the quadrature [69, 70],

$$\hat{X}_\theta(\Omega) \equiv [e^{-i\theta} \hat{b}_{\text{out}}^{(\text{tx})}(\omega_d + \Omega) + e^{i\theta} \hat{b}_{\text{out}}^{(\text{tx})\dagger}(\omega_d - \Omega)]/2 + \text{H.C.}, \quad (67)$$

corresponding to the measured observable of a homodyne measurement of the field $\hat{b}_{\text{out}}^{(\text{tx})}(\omega)$ using a local oscillator with frequency ω_d and phase θ . The power spectral density $S(\Omega)$ for the zero-mean field $\hat{X}_\theta(\Omega)$ is

$$S(\Omega) \delta(\Omega - \Omega') \equiv \langle \hat{X}_\theta(\Omega) \hat{X}_\theta(\Omega') \rangle, \quad (68)$$

and can be directly determined from the results above. As shown in Fig. 7, the resulting outgoing field exhibits squeezing, $S < 1$, for suitable parameters.

VII. OPTICAL IMPEDANCE AND FULL ELECTRO-OPTOMECHANICAL EQUIVALENT CIRCUIT

In Section IV, we derived the equivalent circuit for an AC-driven EM interface involving an arbitrary linear electrical circuit. We now extend the theory to accommodate optomechanical coupling. We consider a single optical cavity mode whose frequency $\omega_{\text{cav}}(\hat{x})$ is modulated by the same mechanical position \hat{x} entering the EM coupling. To this end, we exploit that the OM interface is largely equivalent to the AC-driven EM interface. Following the standard

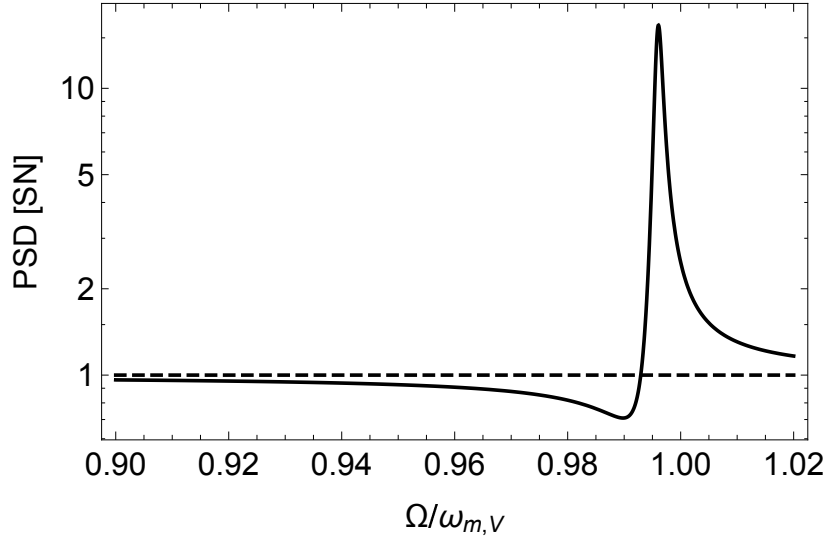


Figure 7. Squeezing of a traveling electro-magnetic field produced by a cold microwave LC resonator ($n_{\text{tx}} \approx 0$, $\bar{\omega}_{\text{LC}} = 2\pi \times 1\text{GHz}$) coupled to a mechanical mode ($\omega_{\text{m},\text{v}} = 2\pi \times 1\text{MHz}$) at an ambient temperature $T_{\text{m}} = 4\text{K}$. Plotted is the homodyne spectrum $S(\Omega)$ of $\hat{X}_\theta(\Omega)$ for a local oscillator phase $\theta \approx 0.18\pi$, which maximizes the squeezing obtainable for a single spectral component (at $\Omega \approx 0.99\omega_{\text{m},\text{v}}$ for these parameters). The shot noise limit at 1 (in the normalization used here) is indicated by the dashed line. Other system parameters used are $Z_{\text{tx}} = 50\Omega$, $Q_{\text{LC}} = \bar{\omega}_{\text{LC}}L/Z_{\text{tx}} = 100$, $\omega_{\text{d}} = \bar{\omega}_{\text{LC}} - 2\pi \times 5\text{MHz}$, $\gamma_{\text{m}} = 2\pi \times 0.1\text{Hz}$, $G/\sqrt{m} = 3.2 \times 10^{11}\text{V}/(\text{m}\sqrt{\text{kg}})$.

procedure [3], we take as our starting point the quantum Hamiltonians for the mechanical and optical modes; the former is given by the quantum analog of Eq. (5) whereas the optical single-mode Hamiltonian is

$$H_{\text{opt}} = \hbar\omega_{\text{cav}}(\hat{x})\hat{a}^\dagger\hat{a}. \quad (69)$$

Applying a coherent optical laser drive of frequency ω_1 to the optical cavity (represented by a Hamiltonian H_1), we expand the total Hamiltonian of the optomechanical system $H = H_{\text{opt}} + H_{\text{m},0} + H_1 + \dots$ around the ensuing steady-state configuration (\bar{x}, α) (where the ellipsis represents the EM coupling and terms responsible for coupling to the environment of the hybrid system). The linearized dynamics of the displaced variables, $\hat{x} = \bar{x} + \delta\hat{x}$ and $\hat{a} = \alpha + \delta\hat{a}$, is then described by the Hamiltonian

$$H_{\text{OM}} = \hbar\bar{\omega}_{\text{cav}}\delta\hat{a}^\dagger\delta\hat{a} + \left[\frac{\delta\hat{p}^2}{2m} + \frac{1}{2}m\omega_{\text{m}}^2\delta\hat{x}^2 \right] + H_{\text{OM,int}} \quad (70)$$

$$H_{\text{OM,int}} \equiv \sqrt{\hbar}G_{\text{OM}}\delta\hat{x}(e^{i\omega_1 t}e^{-i\theta}\delta\hat{a} + e^{-i\omega_1 t}e^{i\theta}\delta\hat{a}^\dagger)/\sqrt{2}, \quad (71)$$

where the first and second terms of Eq. (70) are the “free-evolution” Hamiltonians of the displaced optical and mechanical modes, whereas the third term, $H_{\text{OM,int}}$, is the drive-enhanced linear coupling between them. In the above equations, we have introduced the steady-state cavity resonance $\bar{\omega}_{\text{cav}}$, the optically shifted mechanical frequency ω_{m} , the optomechanical coupling strength G_{OM} (units of $\sqrt{\text{energy} \times \text{frequency}/\text{length}}$), and the phase of the intracavity drive field θ ,

$$\omega_{\text{m}}^2 \equiv \omega_{\text{m},0}^2 + \frac{\hbar|\alpha|^2}{m} \left. \frac{d^2\omega_{\text{cav}}}{dx^2} \right|_{x=\bar{x}}, \quad G_{\text{OM}} \equiv \sqrt{2\hbar} \left. \frac{d\omega_{\text{cav}}}{dx} \right|_{x=\bar{x}} |\alpha|, \quad \theta \equiv \text{Arg}[\alpha]. \quad (72)$$

The coupling strength G_{OM} can be related to the more familiar coupling rate g_{OM} that appear in the conventional form of the coupling Hamiltonian (71),

$$H_{\text{OM,int}} = \hbar g_{\text{OM}}(\delta\hat{c} + \delta\hat{c}^\dagger)(e^{i\omega_1 t}e^{-i\theta}\delta\hat{a} + e^{-i\omega_1 t}e^{i\theta}\delta\hat{a}^\dagger), \quad (73)$$

where $\delta\hat{c}$ is the mechanical bosonic annihilation operator, $[\delta\hat{c}, \delta\hat{c}^\dagger] = 1$. Using $\delta\hat{x} = x_{\text{ZPF}}(\delta\hat{c} + \delta\hat{c}^\dagger)$ and $x_{\text{ZPF}} \equiv \sqrt{\hbar/2m\omega_{\text{m}}}$ and comparing Eqs. (71) and (73), the two optomechanical coupling parameters are seen to be related by

$$g_{\text{OM}} = G_{\text{OM}}/\sqrt{4m\omega_{\text{m}}}. \quad (74)$$

In order to achieve equations of motion equivalent to those governing the EM coupling considered in Section IV, we note that within the rotating wave approximation (RWA), we may approximate the interaction Hamiltonian (71) by

$$H_{\text{OM,int}} \approx \sqrt{\hbar} G_{\text{OM}} \delta \hat{x} (e^{i\omega_1 t} + e^{-i\omega_1 t}) \hat{X}, \quad (75)$$

where we have introduced the dimensionless light quadratures

$$\hat{X} \equiv (e^{-i\theta} \delta \hat{a} + e^{i\theta} \delta \hat{a}^\dagger) / \sqrt{2}, \quad \hat{P} \equiv (e^{-i\theta} \delta \hat{a} - e^{i\theta} \delta \hat{a}^\dagger) / (\sqrt{2}i), \quad (76)$$

obeying $[\hat{X}, \hat{P}] = i$. Note that here we have gone in the opposite direction of what is typically done in the RWA, where expressions similar to Eq. (75) are replaced by Eq. (71). As opposed to electromechanics, where this may not be the case, the RWA is typically a very good approximation in optomechanics since the dynamics on the mechanical timescale $2\pi/\omega_m$ are much slower than that of the optical drive $2\pi/\omega_1$. As a consequence, the derivation of the coupling Hamiltonian (71) assumes the RWA from the outset, and there is a priori no reason to prefer one form over the other. By choosing the form in Eq. (75), however, the Hamiltonian linearly couples $\delta \hat{x}$ to \hat{X} with a strength G_{OM} in a manner similar to the linearized EM interaction Hamiltonian (8) considered above. With the form in Eq. (75), we can thus obtain the equivalent circuit in an analogous way.

We now consider how the optical mode couples to its environment via its loss and drive ports. This can conveniently be treated using the input/output formalism from quantum optics [45], which is analogous to the input/output theory for circuits considered in Section V. In quantum optics, this formalism is traditionally only discussed within the RWA, and the microscopic details of the optical bath coupling is in general not known, leaving it an open question how the bath couples to the quadrature variables (\hat{X}, \hat{P}) [50]. Assuming a linear coupling to the bath modes, the precise microscopic model is, however, unimportant within the RWA. Thus, in a spirit similar to Eq. (75), this permits us to assume that the optical bath modes couple to the quadrature \hat{X} , resulting in the usual viscous damping and noise terms in the equation of motion of the conjugate quadrature \hat{P} (within the Markov approximation)

$$\begin{aligned} \dot{\hat{X}} &= \bar{\omega}_{\text{cav}} \hat{P} \\ \dot{\hat{P}} &= -\bar{\omega}_{\text{cav}} \hat{X} - \kappa \hat{P} + \sqrt{2\kappa} \hat{P}_{\text{in}} + \dots, \end{aligned} \quad (77)$$

where, as previously, a dot above an operator indicates the time derivative, κ is the decay rate of the optical mode, and the operator \hat{P}_{in} represents the noise and/or signal input leaking into the mode (the ellipsis represents OM coupling terms). The input operator \hat{P}_{in} and its output counterpart \hat{P}_{out} can be expanded on a set of itinerant bosonic modes, in analogy to Eq. (60), as

$$\hat{P}_p(t) = \int_0^\infty \frac{d\omega}{\sqrt{2\pi}} \sqrt{\frac{\omega}{\bar{\omega}_{\text{cav}}}} [\hat{a}_p(\omega) e^{-i\omega t} + \hat{a}_p^\dagger(\omega) e^{i\omega t}], \quad (78)$$

where $p \in \{\text{in, out}\}$ and we have introduced bosonic field operators obeying $[\hat{a}_p(\omega), \hat{a}_p^\dagger(\omega')] = \delta(\omega - \omega')$ and $[\hat{a}_p(\omega), \hat{a}_p(\omega')] = 0$. The normalization of Eq. (78) was chosen so as to achieve a simple dimensionless form of Eqs. (77) (resulting in the appearance of the cavity resonance frequency $\bar{\omega}_{\text{cav}}$). If \hat{P}_{in} is in a thermal state then Eq. (78) represents an ohmic bath with the following expectation value in Fourier space ($\omega, \omega' > 0$)

$$\begin{aligned} \langle \hat{P}_{\text{in}}^\dagger(\omega) \hat{P}_{\text{in}}(\omega') \rangle &= \frac{\omega}{\bar{\omega}_{\text{cav}}} n_{\text{opt}}(\omega) \delta(\omega - \omega') \\ \langle \hat{P}_{\text{in}}(\omega) \hat{P}_{\text{in}}^\dagger(\omega') \rangle &= \frac{\omega}{\bar{\omega}_{\text{cav}}} [n_{\text{opt}}(\omega) + 1] \delta(\omega - \omega'), \end{aligned} \quad (79)$$

where n_{opt} is given by Eq. (4) in terms of the temperature of the optical system T_{opt} . For all practical purposes the magnitude of optical frequencies is such that $|\hbar\omega/k_B T_{\text{opt}}| \gg 1$, which entails that to very good approximation we may take the optical noise to be vacuum, $n_{\text{opt}}(\omega) \approx 0$. With the conventions implicit in Eqs. (76)–(78), the optical input-output relation for a single-sided cavity reads (for $\omega > 0$),

$$\hat{a}_{\text{out}}(\omega) = i \sqrt{\frac{\omega}{\bar{\omega}_{\text{cav}}}} \sqrt{\kappa} e^{-i\theta} \hat{a}(\omega) + \hat{a}_{\text{in}}(\omega), \quad (80)$$

where the intracavity drive phase θ was introduced in Eq. (72).

Having achieved OM equations of motion similar to the EM equations, we may straightforwardly retrace the steps of Section IV to derive an OM equivalent circuit. Rather than considering this on its own, we proceed immediately to the transduction scenario with simultaneous electro- and optomechanical couplings. In this case the displaced

variables $\delta Q, \delta x, \delta a$ are defined with respect to the equilibrium configuration of the electro-optomechanical hybrid system subjected to simultaneous electrical and optical driving (we again neglect higher harmonics of the system response). Kirchoff's law for the mechanical loop (37) then generalizes to

$$2V_m(\Omega) = \left[-i\Omega L_m + R_m + \frac{1}{-i\Omega C'_m} \right] I_m(\Omega) + \frac{2I_m(\Omega) + I_{e,+}(\Omega) + I_{e,-}(\Omega)}{-i\Omega \bar{C}_c} + \frac{2I_m(\Omega) + I_{o,+}(\Omega) + I_{o,-}(\Omega)}{-i\Omega \bar{C}_{\text{opt}}}, \quad (81)$$

whereas the effective electrical equations (38) are unaltered, but supplemented by the optical counterparts

$$V_{o,\pm}(\Omega) = Z_{o,\pm}(\Omega)I_{o,\pm}(\Omega) + \frac{I_{o,\pm}(\Omega) + I_m(\Omega)}{-i\Omega \bar{C}_{\text{opt}}} \quad (82)$$

Here we define optical upper/lower sideband quantities $V_{o,\pm}(\Omega), Q_{o,\pm}(\Omega), I_{o,\pm}(\Omega)$ and $Z_{o,\pm}(\Omega)$ analogously to the electrical quantities in Eqs. (33)–(36) with the replacements $\omega_d \rightarrow \omega_1, Z \rightarrow Z_{\text{opt}}, \delta V \rightarrow 2V_{o,\text{in}}, \delta Q \rightarrow \delta Q_o$, and according to the definitions (here and henceforth replacing \hat{X} by its classical counterpart X without loss of generality, see discussion in Section VI)

$$\delta Q_o \equiv \sqrt{\hbar \bar{\omega}_{\text{cav}}} \frac{\bar{C}_c G}{G_{\text{OM}}} X, \quad I_o \equiv \delta \dot{Q}_o \quad (83)$$

$$Z_{\text{opt}}(\omega) = -i\omega L_{\text{opt}} + R_{\text{opt}} \quad (84)$$

$$L_{\text{opt}} \equiv \frac{G_{\text{OM}}^2}{\bar{C}_c^2 G^2 \bar{\omega}_{\text{cav}}^3}, \quad \bar{C}_{\text{opt}} \equiv \bar{\omega}_{\text{cav}} \frac{\bar{C}_c^2 G^2}{G_{\text{OM}}^2}, \quad R_{\text{opt}} \equiv \kappa L_{\text{opt}} \quad (85)$$

and

$$1/C'_m \equiv 1/C_m - 2/\bar{C}_{\text{opt}}. \quad (86)$$

Furthermore, while the mechanical capacitance C_m is still defined by Eq. (24), the mechanical frequency $\omega_{m,V}$ entering this definition now contains static shifts from both the EM and OM interactions, (23) and (72), combining to

$$\omega_{m,V} = \omega_{m,0}^2 - \frac{\langle \bar{Q}_c^2(t) \rangle}{2m\bar{C}_c^2} \frac{d^2 C_c}{dx^2} \Big|_{x=\bar{x}} + \frac{\hbar|\alpha|^2}{m} \frac{d^2 \omega_{\text{cav}}}{dx^2} \Big|_{x=\bar{x}}. \quad (87)$$

Note that the need to define the modified C'_m (86) appearing in Eq. (81), which was not required for the electrical coupling, can be traced to the difference in how we define the coupling constant (whether we take derivatives of the resonance frequency or the capacitance). Converting Eq. (78) to electrical units we obtain the equivalent optical input and output voltage fields ($p \in \{\text{in}, \text{out}\}$)

$$\hat{V}_{o,p}(t) \equiv \sqrt{\frac{\hbar \bar{\omega}_{\text{cav}} R_{\text{opt}}}{2}} \hat{P}_p(t) = \int_0^\infty \frac{d\omega}{\sqrt{2\pi}} \sqrt{\frac{\hbar \omega R_{\text{opt}}}{2}} [\hat{a}_p(\omega) e^{-i\omega t} + \hat{a}_p^\dagger(\omega) e^{i\omega t}], \quad (88)$$

which is completely analogous to Eq. (60). We likewise convert the optical input-output relation (80) into electrical units using Eqs. (76,83,88),

$$V_{o,\text{out}}(\omega) = -R_{\text{opt}} I_o(\omega) + V_{o,\text{in}}(\omega), \quad (89)$$

completely analogous to its electrical counterpart (45) [Eq. (89) is stated in terms of classical variables without loss of generality, see Section VI]. This full set of equations can be represented by the combined electro-optomechanical equivalent circuit diagram shown in Fig. 8, which generalizes Fig. 3.

From the equivalence between the optical mode and the serial RLC, the equations derived for the latter in the last paragraph of Section V carry over straightforwardly to the analogous optical system of a single cavity mode with two decay channels, $\kappa = \kappa_{\text{int}} + \kappa_{\text{ext}}$, where κ_{int} is the intrinsic loss rate and κ_{ext} is the coupling rate to the optical signal port. Hence, the optical impedance is

$$Z_{\text{opt}}(\omega) = -i\omega L_{\text{opt}} + R_{\text{int}} + Z_{\text{ext}}, \quad (90)$$

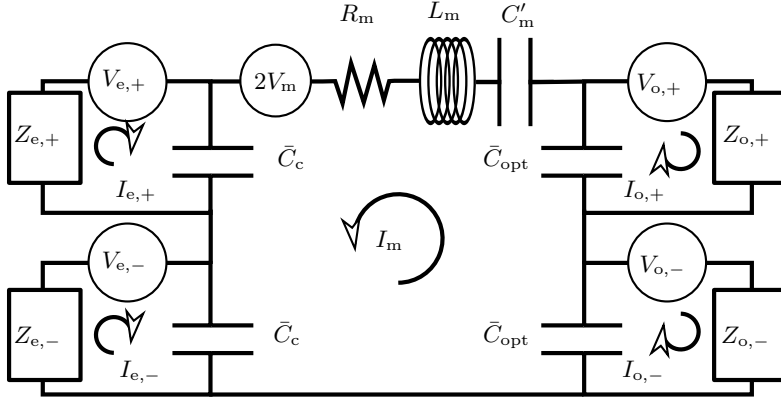


Figure 8. Electro-optomechanical equivalent circuit for a mechanical mode acting as an intermediary between an arbitrary linear electrical circuit and a single optical mode. Each of the electrical or optical sidebands are represented by a loop current $I_{e,\pm}$ or $I_{o,\pm}$ in the diagram and are coupled capacitively to the mechanical loop current I_m via \bar{C}_c or \bar{C}_{opt} . The effective voltage sources $V_{e,\pm}, V_{o,\pm}, V_m$ represent electrical, optical, and mechanical noise or signal inputs. Using standard circuit rules to determine the current in an external loop, we may determine the output at the corresponding sideband.

where we use Eq. (85) to define $R_{int} \equiv \kappa_{int} L_{opt}$, $Z_{ext} \equiv \kappa_{ext} L_{opt}$. Similar to Eqs. (46,47), we have the optical coupling efficiency

$$\eta_{opt} \equiv Z_{ext}/(R_{int} + Z_{ext}) = \kappa_{ext}/(\kappa_{int} + \kappa_{ext}). \quad (91)$$

Accordingly, the equivalent optical input and output voltages $V_{o,in/out}$ each split into two independent contributions of the same form (88) obtained by the replacements $R_{opt} \rightarrow R_{int}, Z_{ext}$, respectively, and introducing appropriate bosonic operators. Analogously, the optical readout is found by reexpressing Eq. (89) in terms of the upper and lower sideband optical currents $I_{o,\pm}(\Omega)$ ($\Omega > 0$)

$$V_{o,out}^{(ext)}(\omega_1 + \Omega) = -\frac{\omega_1 + \Omega}{\Omega} Z_{ext} I_{o,+}(\Omega) + V_{o,in}^{(ext)}(\omega_1 + \Omega) \quad (92)$$

$$V_{o,out}^{(ext)}(\omega_1 - \Omega) = \frac{\omega_1 - \Omega}{\Omega} Z_{ext} I_{o,-}^*(\Omega) + V_{o,in}^{(ext)}(\omega_1 - \Omega). \quad (93)$$

Considering the electro-optomechanical circuit diagram (Fig. 8), we are led to define the mechanical impedance in the presence of OM coupling (cf. Eq. (10)),

$$Z'_m(\Omega) \equiv -i\Omega L_m + R_m + \frac{1}{-i\Omega C'_m}, \quad (94)$$

and observe that the central loop in Fig. 8 has an effective impedance (cf. Eq. (51))

$$Z_{m,eff}(\Omega) = Z'_m(\Omega) + \Delta Z(\Omega), \quad (95)$$

where the latter term represents the four parallel connections. Applying standard impedance combination rules we find (generalizing Eq. (52)),

$$\Delta Z(\Omega) = \sum_l [-i\Omega C_l + 1/Z_l(\Omega)]^{-1} = \frac{1}{-i\Omega} \sum_{s=\pm} \left(\frac{1 + \mathcal{Q}_{e,s}(\Omega)}{\bar{C}_c} + \frac{1 + \mathcal{Q}_{o,s}(\Omega)}{\bar{C}_{opt}} \right), \quad (96)$$

where the optical susceptibility functions are defined in analogy to their electrical counterparts (53),

$$\mathcal{Q}_{o,\pm}(\Omega) \equiv -\frac{1}{1 - i\Omega \bar{C}_{opt} Z_{o,\pm}(\Omega)}. \quad (97)$$

The resulting effective impedance $Z_{m,eff}$ (95) captures the dynamical back-action modifications to the mechanical response induced by each of the sideband couplings. The effective mechanical resonance frequency Ω_m , including all static and dynamical shifts from the electrical and optical interactions, can be found from Eq. (96) as the solution to the equation (assuming we are below the threshold for normal-mode splitting [71])

$$\text{Im}[Z_{m,eff}(\Omega_m)] = 0, \quad (98)$$

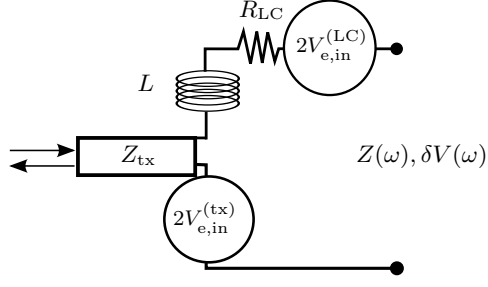


Figure 9. The electrical part of the example hybrid system [Fig. 1] that determines the Thévenin equivalent quantities $Z(\omega)$ and $\delta V(\omega)$. Note that the subcircuit does not include the coupling capacitor.

leading us to define the effective mechanical resistance

$$R_{m,\text{eff}} \equiv Z_{m,\text{eff}}(\Omega_m), \quad (99)$$

which yields the effective transducer bandwidth $\gamma_{m,\text{eff}} \equiv R_{m,\text{eff}}/L_m$ in the weak-coupling regime.

VIII. EXAMPLE OF APPLICATION

To demonstrate the full electro-optomechanical circuit formalism we now consider a specific example of a transducer. We choose the simple scenario of a single mechanical mode serving as the intermediary between a serial RLC circuit via its capacitance $C_c(x)$ and a single mode of an optical cavity via a parametric dispersive coupling, see Figs. 1 and 9. Other electrical circuit layouts will be considered elsewhere [72].

We note that the current responses of the various sideband loops $I_l(\Omega)$ to the input fields can be determined by straightforward generalization of Eq. (55). Combining these with the input-output relations (49,50,92,93) yields the scattering matrix between the sidebands of the electrical and optical transmission lines (as well as the noise sources). Let us for specificity evaluate the optical output at the upper sideband (92) at the effective mechanical peak frequency Ω_m defined in Eq. (98), assuming red-detuned driving for both the optical and electrical subsystems $\bar{\omega}_{LC} - \omega_d = \Omega_m = \bar{\omega}_{\text{cav}} - \omega_l$. The current response of interest $I_{o,+}$ depends on the susceptibility functions (53,97), which at the mechanical peak take the values

$$\mathcal{Q}_{o,+}(\Omega_m) = -iQ_{\text{cav}}, \quad \mathcal{Q}_{o,-}(\Omega_m) \approx \frac{iQ_{\text{cav}}}{1 - 4iQ_{\text{cav}}\Omega_m/\bar{\omega}_{\text{cav}}} \quad (100)$$

$$\mathcal{Q}_{e,+}(\Omega_m) = -iQ_{LC}, \quad \mathcal{Q}_{e,-}(\Omega_m) \approx \frac{iQ_{LC}}{1 - 4iQ_{LC}\Omega_m/\bar{\omega}_{LC}}, \quad (101)$$

where $Q_{\text{cav}} \equiv \bar{\omega}_{\text{cav}}/\kappa$ and $Q_{LC} \equiv \bar{\omega}_{LC}L/(R_{LC} + Z_{tx})$ are the loaded quality factors of the optical and electrical resonances, respectively; the approximations are valid in the limit of high quality factors $Q_{\text{cav}}, Q_{LC} \gg 1$ and small mechanical frequency $\Omega_m \ll \bar{\omega}_{\text{cav}}, \bar{\omega}_{LC}$. These quantities signify the signal enhancement of the various sidebands. Let us, for simplicity, assume the optomechanically resolved-sideband regime, $\kappa/(4\Omega_m) \ll 1$. From Eq. (100) we see that this implies that $|\mathcal{Q}_{o,-}(\Omega_m)/\mathcal{Q}_{o,+}(\Omega_m)| \ll 1$ and hence we may disregard the loop (o,-) altogether (although for applications where quantum noise is important, one has to carefully consider to what extent this limit is fulfilled [62]). In this scenario, we arrive at a scattering relation of the form

$$\hat{a}_{\text{out}}^{(\text{ext})}(\bar{\omega}_{\text{cav}}) = S_{\text{tx},+}\hat{b}_{\text{in}}^{(\text{tx})}(\bar{\omega}_{LC}) + S_{LC,+}\hat{b}_{\text{in}}^{(LC)}(\bar{\omega}_{LC}) + S_{\text{tx},-}\hat{b}_{\text{in}}^{(\text{tx})\dagger}(\bar{\omega}_{LC} - 2\Omega_m) + S_{LC,-}\hat{b}_{\text{in}}^{(LC)\dagger}(\bar{\omega}_{LC} - 2\Omega_m) + S_m\hat{c}_{\text{in}}(\Omega_m) + S_{\text{ext},+}\hat{a}_{\text{in}}^{(\text{ext})}(\bar{\omega}_{\text{cav}}) + S_{\text{int},+}\hat{a}_{\text{in}}^{(\text{int})}(\bar{\omega}_{\text{cav}}), \quad (102)$$

where $\hat{a}_{\text{in}}^{(X)}, \hat{b}_{\text{in}}^{(X)}, \hat{c}_{\text{in}}^{(X)}$ are optical, electrical, and mechanical input operators, respectively. Using the dimensionless voltage mapping factor ζ from the mechanical loop to the upper optical sideband,

$$\zeta \equiv -2\frac{\bar{\omega}_{\text{cav}}}{\Omega_m}Z_{\text{ext}}\frac{-iQ_{\text{cav}}}{R_{m,\text{eff}}} = i\eta_{\text{opt}}\frac{4g_{\text{OM}}^2}{\bar{\omega}_{\text{cav}}\gamma_{m,\text{eff}}}, \quad (103)$$

expressed in terms of $g_{\text{OM}} = G_{\text{OM}}/\sqrt{4m\Omega_m}$ and $\gamma_{\text{m,eff}}$, defined below Eq. (99), the scattering matrix elements are

$$S_{\text{m}} = \zeta \sqrt{\frac{\Omega_m R_{\text{m}}}{\bar{\omega}_{\text{cav}} Z_{\text{ext}}}} \quad (104)$$

$$S_{\text{tx},+} = \zeta \sqrt{\frac{\bar{\omega}_{\text{LC}} Z_{\text{tx}}}{\bar{\omega}_{\text{cav}} Z_{\text{ext}}}} \mathcal{Q}_{\text{e},+}(\Omega_m) \quad S_{\text{tx},-} = \zeta \sqrt{\frac{(\bar{\omega}_{\text{LC}} - 2\Omega_m) Z_{\text{tx}}}{\bar{\omega}_{\text{cav}} Z_{\text{ext}}}} \mathcal{Q}_{\text{e},-}(\Omega_m) \quad (105)$$

$$S_{\text{LC},+} = \zeta \sqrt{\frac{\bar{\omega}_{\text{LC}} R_{\text{LC}}}{\bar{\omega}_{\text{cav}} Z_{\text{ext}}}} \mathcal{Q}_{\text{e},+}(\Omega_m) \quad S_{\text{LC},-} = \zeta \sqrt{\frac{(\bar{\omega}_{\text{LC}} - 2\Omega_m) R_{\text{LC}}}{\bar{\omega}_{\text{cav}} Z_{\text{ext}}}} \mathcal{Q}_{\text{e},-}(\Omega_m) \quad (106)$$

$$S_{\text{ext},+} = 1 - 2\eta_{\text{opt}} - iQ_{\text{cav}}\zeta \quad S_{\text{int},+} = \sqrt{\eta_{\text{opt}}^{-1} - 1} [-2\eta_{\text{opt}} - iQ_{\text{cav}}\zeta], \quad (107)$$

where $\mathcal{Q}_{\text{e},\pm}(\Omega_m)$ are given in Eqs. (101). All of the scattering elements contain a frequency and impedance conversion factor of the form $\sqrt{\omega_{\text{in}} R_{\text{in}}/\omega_{\text{out}} R_{\text{out}}}$; this is merely the ratio of conversion factors between voltage and the itinerant bosonic modes. The electrical and mechanical scattering coefficients (104)–(106) only consist of single terms because for these sources only a single path exists to the optical readout port 'ext'. In contrast, the effective reflection coefficient for the 'ext' port $S_{\text{ext},+}$ (107) results from interference of various scattering paths.

A useful characterization of the transducer can be given in terms of its signal transfer efficiency η and its added noise flux per unit bandwidth N (referenced to the input [62]). These are readily extracted from the scattering matrix. As we are considering signal conversion from the upper optical sideband to the upper electrical sideband, the (peak) signal transfer efficiency is

$$\eta = |S_{\text{tx},+}|^2 = 4 \frac{\eta_{\text{el}} \eta_{\text{opt}}}{R_{\text{m,eff}}^2} \frac{Q_{\text{LC}}}{\Omega_m \bar{C}_c} \frac{Q_{\text{cav}}}{\Omega_m \bar{C}_{\text{opt}}}. \quad (108)$$

The added flux of noise quanta per unit bandwidth N contaminating the output at the upper optical sideband, referenced to the input, is $N(\omega)\delta(\omega - \omega') = \eta^{-1} \langle \hat{a}_{\text{out}}^{(\text{ext})\dagger}(\omega) \hat{a}_{\text{out}}^{(\text{ext})}(\omega') \rangle \Big|_{\text{no signal}}$, where the input at the signal port is disregarded since it is considered as signal and not noise. For our scattering relation we find from Eqs. (102)–(107) that at the transducer peak the added noise is

$$N = \frac{1}{\eta_{\text{el}}} \frac{R_{\text{m}} \Omega_m \bar{C}_c}{Q_{\text{LC}}} n_{\text{m}}(\Omega_m) + \left(\frac{1}{\eta_{\text{el}}} - 1 \right) n_{\text{LC}}(\bar{\omega}_{\text{LC}}) + \left(1 + \left[\frac{4\Omega_m L}{R_{\text{LC}} + Z_{\text{tx}}} \right]^2 \right)^{-1} \left[\left(\frac{1}{\eta_{\text{el}}} - 1 \right) (n_{\text{LC}}(\bar{\omega}_{\text{LC}} - 2\Omega_m) + 1) + (n_{\text{tx}}(\bar{\omega}_{\text{LC}} - 2\Omega_m) + 1) \right]. \quad (109)$$

In Eq. (109) we see that in this case the electrical added noise is only affected by η_{el} for the upper sideband (term proportional to $n_{\text{LC}}(\bar{\omega}_{\text{LC}})$), whereas for the lower sideband (second line), the noise is further suppressed by the degree to which the sideband is off-resonant from the RLC resonator. Also this term has extra vacuum noise contributions (unity terms added to n_{LC} and n_{tx}) since it stems from the lower sideband (i.e., from $\hat{b}_{\text{in}}^{(X)\dagger}$). Turning to the mechanical contribution $\propto n_{\text{m}}$, the suppression factor is $1/(\eta_{\text{el}} \mathcal{C}_{\text{EM}})$, where we have introduced the EM cooperativity,

$$\mathcal{C}_{\text{EM}} \equiv Q_{\text{LC}}/(R_{\text{m}} \Omega_m \bar{C}_c) = 4g_{\text{EM}}^2/(\gamma_{\text{LC}} \gamma_{\text{m},0}), \quad (110)$$

in terms of LC linewidth $\gamma_{\text{LC}} \equiv R_{\text{LC}}/L$ and the EM coupling rate $g_{\text{EM}} = G/\sqrt{4mL\Omega_m \bar{\omega}_{\text{LC}}}$ between annihilation operators (analogous to its OM counterpart (74)). This reduction in the mechanical noise is a consequence of the EM signal rate overwhelming the intrinsic mechanical decay rate by the factor $\eta_{\text{el}} \mathcal{C}_{\text{EM}}$. Since we have assumed the OM resolved-sideband regime and are driving optically red-detuned, the contribution to N from the optical vacuum inputs vanish. The scenario considered here can also be seen as a cascade of three coupled oscillators for which the results have also been derived elsewhere [35, 73, 74]. We stress, however, that the formalism allows for the analysis of arbitrary linear circuits.

IX. ADIABATIC ELIMINATION OF ELECTRICAL AND OPTICAL MODES

In the preceding sections, we have demonstrated how the electro-optomechanical equivalent circuit in Fig. 8 can be used to deduce the elements of the scattering matrix. However, if the effective mechanical linewidth is narrow

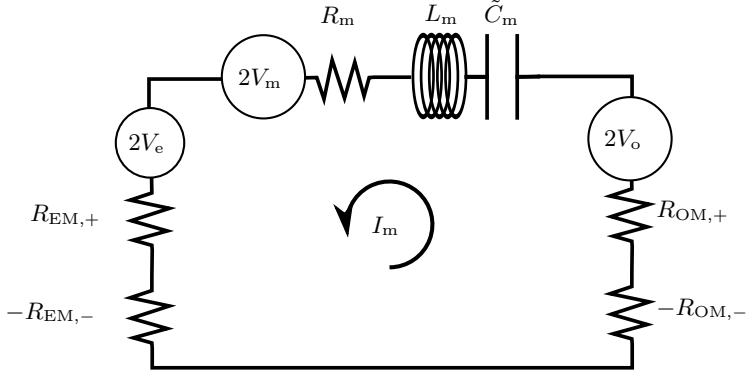


Figure 10. Reduced electro-optomechanical equivalent circuit in which electrical and optical modes have been adiabatically eliminated. It consists of an effective mechanical loop of shifted resonance frequency loaded by a resistive element for each sideband coupling. The resistances are positive for the upper sidebands, $R_{EM/OM,+}$, and negative for the lower ones, $-R_{EM/OM,-}$, leading to amplification effects. Each sideband coupling drives the effective mechanical loop with a Thévenin voltage representing the noise and signal ports of that subsystem. The readout of the system corresponds to the signal dissipated in the various ports.

compared to the other electrical and optical subsystems, we may derive an even simpler, reduced equivalent circuit (Fig. 10) by adiabatically eliminating the electrical and optical modes in Fig. 8. Such elimination amounts, in the context of complex impedances, to neglecting the weak frequency dependence of the electrical and optical loads on the mechanical mode as given by Eq. (96).

We start by expressing the effective mechanical resonance frequency,

$$\Omega_m \equiv \frac{1}{L_m \tilde{C}_m}, \quad (111)$$

including dynamical shifts from the coupling to electrical and optical subsystems in terms of an effective mechanical capacitance \tilde{C}_m . The frequency Ω_m was defined in Eq. (98), but here we will evaluate it perturbatively. To zeroth order in $\mathcal{Q}_{i,\pm}$, we have $\Omega_m = \omega_{m,Q}$ from Eqs. (94-96,98); we therefore approximate the shift from $\mathcal{Q}_{i,\pm}(\Omega)$ by evaluating it at this frequency, yielding the effective mechanical capacitance

$$\frac{1}{\tilde{C}_m} = \frac{1}{C_m} + \frac{2}{\tilde{C}_c} + \frac{1}{\tilde{C}_c} (\text{Re}[\mathcal{Q}_{e,+}(\omega_{m,Q}) + \mathcal{Q}_{e,-}(\omega_{m,Q})]) + \frac{1}{\tilde{C}_{\text{opt}}} (\text{Re}[\mathcal{Q}_{o,+}(\omega_{m,Q}) + \mathcal{Q}_{o,-}(\omega_{m,Q})]), \quad (112)$$

where we have replaced C'_m with the original C_m using Eq. (86). Note that the sum of the two first terms of Eq. (112) corresponds to the frequency $\omega_{m,Q}$ (as per Eq. (21) with an extra factor of 2 in front of $1/\tilde{C}_c$ in the AC case as stated below Eq. (31)). In the following, we will derive the effective resistive loads imposed on the mechanical mode.

A. Elimination of optical mode

The real part of the OM load from the respective sidebands give rise to effective resistive elements $\pm R_{EM,\pm}$. Evaluating the relevant parts of Eq. (96) at the mechanical frequency $\omega_{m,Q}$, we find

$$R_{OM,\pm} \equiv \pm \text{Re} \left[\frac{\mathcal{Q}_{o,\pm}(\Omega)}{-i\Omega \tilde{C}_{\text{opt}}} \right] \Bigg|_{\Omega=\omega_{m,Q}}. \quad (113)$$

This can be put on a more specific form since we are assuming a single cavity mode throughout this work, thus fixing the form of the optical impedance Z_{opt} (84). Considering optical frequencies ω close to the cavity resonance, $|\omega - \bar{\omega}_{\text{cav}}| \ll \bar{\omega}_{\text{cav}}$, the optical susceptibility $\mathcal{Q}_{o,\pm}(\Omega)$ is well-approximated by a Lorentzian. Ignoring corrections of order $\omega_{m,Q}/\omega_1$, this allows us to reexpress Eq. (113) as

$$R_{OM,\pm} = L_m \gamma_{OM,\pm} \quad (114)$$

$$\gamma_{OM,\pm} \equiv \gamma_{m,0} \mathcal{C}_{OM} \mathcal{L}_{\pm}^2, \quad \mathcal{C}_{OM} \equiv \frac{4g_{OM}^2}{\gamma_{m,0}\kappa}, \quad (115)$$

where $\gamma_{\text{OM},\pm}$ are the OM anti-Stokes and Stokes rates expressed in terms of the OM cooperativity \mathcal{C}_{OM} and the Lorentzian sideband strengths \mathcal{L}_{\pm} at the upper/lower OM sidebands,

$$\mathcal{L}(\omega) \equiv \frac{\kappa/2}{-i(\omega - \bar{\omega}_{\text{cav}}) + \kappa/2}, \quad (116)$$

$$\mathcal{L}_{\pm} \equiv |\mathcal{L}(\omega_1 \pm \omega_{\text{m},Q})|, \quad \theta_{\pm} \equiv \text{Arg}[\mathcal{L}(\omega_1 \pm \omega_{\text{m},Q})], \quad (117)$$

also introducing the sideband phases θ_{\pm} . The effective optical Thévenin voltage V_{o} , which has contributions from $V_{\text{o},\pm}$, can be determined by voltage division (see discussion above Eq. (55)),

$$V_{\text{o}}(\Omega) \approx -iQ_{\text{cav}}[e^{i\theta_+}\mathcal{L}_+V_{\text{o},+}(\Omega) - e^{-i\theta_-}\mathcal{L}_-V_{\text{o},-}(\Omega)], \quad (118)$$

where we have ignored the frequency dependence of $\mathcal{L}(\omega)$ over the bandwidth of interest as in Eq. (115). For the typical example of an optical mode with two decay channels considered in Section VIII, $V_{\text{o}}(\Omega)$ in Eq. (118) can be stated explicitly in terms of the bosonic operators of the itinerant optical fields (again ignoring corrections of order $\omega_{\text{m},Q}/\omega_1$),

$$\hat{V}_{\text{o}}(\Omega) \approx -i\frac{2g_{\text{OM}}}{\sqrt{\kappa}}\frac{\sqrt{\hbar m\omega_{\text{m},Q}/2}}{C_c G}[e^{i\theta_+}\mathcal{L}_+\hat{a}_{\text{in}}(\omega_1 + \Omega) - e^{-i\theta_-}\mathcal{L}_-\hat{a}_{\text{in}}^\dagger(\omega_1 - \Omega)], \quad (119)$$

where $\hat{a}_{\text{in}}(\omega) = \sqrt{\eta_{\text{opt}}}\hat{a}_{\text{in}}^{(\text{ext})}(\omega) + \sqrt{1 - \eta_{\text{opt}}}\hat{a}_{\text{in}}^{(\text{int})}(\omega)$ is a linear combination of the two optical input fields. The effective OM input-output relation can be found by combining Eq. (89) with Eq. (82) and the optical counterparts of Eq. (35). For the readout port 'ext' we find the outgoing field

$$a_{\text{out}}^{(\text{ext})}(\omega_1 + \Omega) = ie^{i\theta_+}\sqrt{\eta_{\text{opt}}}\sqrt{\frac{2R_{\text{OM},+}\omega_{\text{m},Q}}{\hbar\omega_{\text{m},Q}}}\frac{I_{\text{m}}(\Omega)}{\Omega} + a_{\text{in}}^{(\text{eff})}(\omega_1 + \Omega) \quad (120)$$

$$a_{\text{out}}^{(\text{ext})}(\omega_1 - \Omega) = -ie^{i\theta_-}\sqrt{\eta_{\text{opt}}}\sqrt{\frac{2R_{\text{OM},-}\omega_{\text{m},Q}}{\hbar\omega_{\text{m},Q}}}\frac{I_{\text{m}}^*(\Omega)}{\Omega} + a_{\text{in}}^{(\text{eff})}(\omega_1 - \Omega), \quad (121)$$

where we have defined the effective optical noise operator ($\Omega > 0$)

$$\hat{a}_{\text{in}}^{(\text{eff})}(\omega_1 \pm \Omega) \equiv [1 - 2\eta_{\text{opt}}\mathcal{L}_{\pm}e^{i\theta_{\pm}}]\hat{a}_{\text{in}}^{(\text{ext})}(\omega_1 \pm \Omega) - 2\sqrt{\eta_{\text{opt}}(1 - \eta_{\text{opt}})}\mathcal{L}_{\pm}e^{i\theta_{\pm}}\hat{a}_{\text{in}}^{(\text{int})}(\omega_1 \pm \Omega). \quad (122)$$

B. Elimination of electrical modes

We define the effective EM resistances from Eq. (96) analogously to Eq. (113),

$$R_{\text{EM},\pm} \equiv \pm \text{Re} \left[\frac{\mathcal{Q}_{e,\pm}(\Omega)}{-i\Omega\bar{C}_c} \right] \Big|_{\Omega=\omega_{\text{m},Q}}. \quad (123)$$

From this expression we find (neglecting corrections of order $\omega_{\text{m},Q}/\omega_{\text{d}}$)

$$R_{\text{EM},\pm} \approx \frac{\omega_{\text{d}}}{\omega_{\text{m},Q}} \text{Re} \left[(-i\omega\bar{C}_c + 1/Z(\omega))^{-1} \right] \Big|_{\omega=\omega_{\text{d}}\pm\omega_{\text{m},Q}}, \quad (124)$$

where $Z(\omega)$ is the arbitrary impedance illustrated in Fig. 3a, here entering in a parallel combination with the coupling capacitor impedance. The Thévenin voltage V_{e} of the reduced circuit (Fig. 10) is easily derived in terms of the Thévenin voltages $V_{\text{e},\pm}$ of Fig. 8 (paralleling Eq. (118)),

$$2V_{\text{e}}(\Omega) \equiv \mathcal{Q}_{e,+}(\omega_{\text{m},Q})V_{\text{e},+}(\Omega) + \mathcal{Q}_{e,-}(\omega_{\text{m},Q})V_{\text{e},-}(\Omega). \quad (125)$$

For purposes of practical calculation, however, a simpler strategy is to calculate V_{e} directly without the intermediate step of determining $V_{\text{e},\pm}$. To this end, note that the contributions of the individual loops l to the effective electro-optical load ΔZ (96) are simply the Thévenin impedances of those loops *including* their respective coupling capacitors. Specifically, denoting the corresponding (lab frame) Thévenin voltage for the electrical circuit $\delta V'(\omega)$, the electrical Thévenin voltage of the reduced equivalent circuit is

$$2V_{\text{e}}(\Omega) = \delta V'(\omega_{\text{d}} + \Omega) + \delta V'^*(\omega_{\text{d}} - \Omega). \quad (126)$$

The effective EM input-output relations can then be determined as in the OM case once the electrical circuit has been specified.

Recapitulating the effective description that we have now obtained (see Fig. 10): The electrical and optical modes enter as effective loads attached to the mechanical loop. The combined electrical and optical loading of the mechanical current loop $\Delta Z(\Omega)$ was derived in Eq. (96). The real part of $\Delta Z(\Omega)$ adds resistance while the imaginary part shifts the mechanical resonance frequency. The effective resistance of the mechanical loop thus has a contribution from each sideband of each coupled subsystem, positive from the upper sidebands and negative for the lower ones

$$R_{m,\text{eff}} = R_m + R_{\text{EM},+} - R_{\text{EM},-} + R_{\text{OM},+} - R_{\text{OM},-}. \quad (127)$$

The resistances $R_{\text{EM}/\text{OM},\pm}$ are the electrical equivalents of the EM/OM anti-Stokes and Stokes rates for the scattering of mechanical phonons into the respective sidebands as electrical/optical photons,

$$\gamma_{\text{EM}/\text{OM},\pm} \equiv R_{\text{EM}/\text{OM},\pm}/L_m. \quad (128)$$

Moreover, each of the eliminated electrical and optical subsystems contribute a voltage source, $V_e(\Omega)$ and $V_o(\Omega)$, to the effective mechanical loop.

As a particular example we again consider a mechanical mode coupled to a serial RLC circuit and a single optical mode [Fig. 1] and derive the reduced equivalent circuit. For specificity, we take both the electrical and optical drives to be red-detuned by $\omega_{m,Q}$. First we determine the effective mechanical resonance frequency Ω_m (111) within the Lorentzian approximation (100,101) as the solution to the equation

$$\Omega_m^2 = \omega_{m,Q}^2 - \frac{\bar{C}_c G^2}{m} \frac{4Q_{\text{LC}}^2 \Omega_m / \bar{\omega}_{\text{LC}}}{1 + (4Q_{\text{LC}} \Omega_m / \bar{\omega}_{\text{LC}})^2} - \frac{G_{\text{OM}}^2}{m \bar{\omega}_{\text{cav}}} \frac{4Q_{\text{cav}}^2 \Omega_m / \bar{\omega}_{\text{cav}}}{1 + (4Q_{\text{cav}} \Omega_m / \bar{\omega}_{\text{cav}})^2}. \quad (129)$$

A perturbative solution to Eq. (129) can be obtained by substituting $\Omega_m \rightarrow \omega_{m,Q}$ on its right-hand side, which amounts to applying the result (112). This determines the frequency at which the mechanical response is maximal (in the limit of high effective mechanical quality factor $Q_{m,\text{eff}} \equiv \Omega_m L_m / R_{m,\text{eff}} \gg 1$) and hence typically the desirable (center) frequency for signal input (in the rotating frame of the drive fields). Next, we determine the resistances $R_{\text{OM},\pm}, R_{\text{EM},\pm}$ from Eqs. (113,123) again making use of the sideband strengths (100,101)

$$R_{\text{OM},+} = \frac{Q_{\text{cav}}}{\omega_{m,Q} \bar{C}_{\text{opt}}}, \quad R_{\text{OM},-} = \frac{Q_{\text{cav}}}{\omega_{m,Q} \bar{C}_{\text{opt}}} \frac{1}{1 + (4Q_{\text{cav}} \omega_{m,Q} / \bar{\omega}_{\text{cav}})^2} \quad (130)$$

$$R_{\text{EM},+} = \frac{\bar{\omega}_{\text{LC}}}{\omega_{m,Q}} \frac{L/\bar{C}_c}{R_{\text{LC}} + Z_{\text{tx}}}, \quad R_{\text{EM},-} = \frac{\bar{\omega}_{\text{LC}}}{\omega_{m,Q}} \frac{L/\bar{C}_c}{R_{\text{LC}} + Z_{\text{tx}}} \frac{1}{1 + (4Q_{\text{LC}} \omega_{m,Q} / \bar{\omega}_{\text{LC}})^2}. \quad (131)$$

The optical and electrical Thévenin voltages of the reduced equivalent circuit are given respectively by Eq. (119) and, using Eqs. (125,101,33), we find

$$2V_e(\Omega) \approx -iQ_{\text{LC}} \delta V(\omega_d + \Omega) + \frac{iQ_{\text{LC}}}{1 - 4iQ_{\text{LC}} \omega_{m,Q} / \bar{\omega}_{\text{LC}}} \delta V^*(\omega_d - \Omega). \quad (132)$$

In view of Eqs. (130,131) and (108), the peak transfer efficiency between the upper sidebands can in our example case be compactly expressed as

$$\eta = \eta_{\text{el}} \eta_{\text{opt}} \frac{4R_{\text{OM},+} R_{\text{EM},+}}{R_{m,\text{eff}}^2}, \quad (133)$$

where the effective mechanical resistance $R_{m,\text{eff}}$ is given by Eq. (127). The reduced equivalent circuit [Fig. 10] with parameters given by Eqs. (111,119,129-132) provides a simplified description of the example hybrid system [Fig. 1] which is accurate for frequency components Ω in a band around Ω_m much narrower than the frequency scale over which the effective electro-optical load $\Delta Z(\Omega)$ (96) varies, i.e., $|\Omega - \Omega_m| \ll \min\{(R_{\text{LC}} + Z_{\text{tx}})/L, \kappa\}$ for the present example. The exact description is recovered by retaining the Ω -dependence of the electrical and optical susceptibility functions $Q_{i,\pm}(\Omega)$ and (consequently) that of the electro-optical load $\Delta Z(\Omega)$.

X. CONCLUSION AND OUTLOOK

Electro-optomechanical hybrid systems are promising candidates for providing low-noise transduction between the electrical and optical domains with applications both in the classical and quantum regime. To fully realize the

technological potential of such hybrid systems, a common framework unifying their disparate components is needed. In this article we have developed an equivalent circuit formalism for electro-optomechanical transduction which is an exact mapping of the linearized dynamics of the hybrid system. This allows the scattering matrix of the transducer to be determined by standard circuit analysis. Importantly, the formalism accommodates AC-driven interfaces and incorporate amplification effects due to finite sideband resolution. This makes the formalism particularly useful for describing transduction between different frequencies. The equivalent circuit description is, however, also applicable when considering scenarios involving only EM or OM components and may help provide a more intuitive understanding of these systems.

Importantly, the framework developed here provides a common language that bridges the gap between the electrical engineering and quantum optics communities. In particular, it allows the engineering community to readily explore the prospects of integrating OM functionalities into electrical systems using the vast set of tools available for circuit design. In this way, one can exploit the low-noise sensing capabilities and optical communication compatibility of optomechanics [34] in real-world applications such as nuclear magnetic resonance (NMR) detection [43] and radio-astronomy.

Our formalism captures the quantum mechanical aspects of transduction in a simple manner and one only has to account for the quantum noise in the input and output. This means that describing the quantum mechanical properties of the device is not more complicated than describing the classical dynamics of the system. The formalism is therefore highly suited for assessing the potential of electro-optomechanical transducers in future quantum communication based on optical networks [75].

The transduction is treated as a scattering scenario, where asymptotic input fields are mapped to output fields. In essence, this means that we consider the source of the signal to be at the other end of an infinitely long transmission line such that it experiences no back action from the transducer. For some transduction applications, such as the conversion of a signal from a superconducting qubit to an optical photon, it may be an advantage to consider a more integrated structure where the qubit is an integral part of the electrical circuit. In such situation, one can envision combining the impedance description of OM systems presented here with the quantum theory of nonlinear circuits, e.g., superconducting flux [76] or charge [77] qubits, or one may use a black-box quantization approach for weakly anharmonic circuits [78] to obtain an efficient description of the joint system.

ACKNOWLEDGMENTS

We acknowledge helpful discussions with A. Simonsen, K. Lehnert, J. Aumentado, R. Simmonds, and K. Usami. We thank J. Foley for reading the manuscript. EZ thanks the JQI for hosting him. JMT thanks the NBI for their hospitality during his many stays.

The research leading to these results was funded by The European Union Seventh Framework Programme through SIQS (grant no. 600645), ERC Grants QIOS (grant no. 306576), and by the European Union's Horizon 2020 research and innovation programme (ERC project Q-CEOM, grant agreement no. 638765 and project HOT, grant agreement no. 732894), a starting grant from the Danish Council for Independent Research (grant number 4002-00060) as well as the Physics Frontier Center at the JQI, DARPA DSO. EZ acknowledges funding from the Carlsberg Foundation.

-
- [1] N. Gisin, G. Ribordy, W. Tittel, and H. Zbinden, *Rev. Mod. Phys.* **74**, 145 (2002).
 - [2] H. J. Kimble, *Nature* **453**, 1023 (2008).
 - [3] M. Aspelmeyer, T. J. Kippenberg, and F. Marquardt, *Rev. Mod. Phys.* **86**, 1391 (2014).
 - [4] M. Aspelmeyer, T. J. Kippenberg, and F. Marquardt, eds., *Cavity Optomechanics: Nano- and Micromechanical Resonators Interacting with Light*, 1st ed., Quantum Science and Technology (Springer-Verlag Berlin Heidelberg, 2014).
 - [5] S. L. Danilishin and F. Y. Khalili, *Living Reviews in Relativity* **15** (2012), 10.12942/lrr-2012-5.
 - [6] O. Arcizet, P. F. Cohadon, T. Briant, M. Pinard, and A. Heidmann, *Nature* **444**, 71 (2006).
 - [7] A. Schliesser, P. Del'Haye, N. Nooshi, K. J. Vahala, and T. J. Kippenberg, *Phys. Rev. Lett.* **97**, 243905 (2006).
 - [8] S. Gigan, H. R. Bohm, M. Paternostro, F. Blaser, G. Langer, J. B. Hertzberg, K. C. Schwab, D. Bauerle, M. Aspelmeyer, and A. Zeilinger, *Nature* **444**, 67 (2006).
 - [9] J. D. Thompson, B. M. Zwickl, A. M. Jayich, F. Marquardt, S. M. Girvin, and J. G. E. Harris, *Nature* **452**, 72 (2008).
 - [10] D. J. Wilson, C. A. Regal, S. B. Papp, and H. J. Kimble, *Phys. Rev. Lett.* **103**, 207204 (2009).
 - [11] J. Chan, T. P. M. Alegre, A. H. Safavi-Naeini, J. T. Hill, A. Krause, S. Groblacher, M. Aspelmeyer, and O. Painter, *Nature* **478**, 89 (2011).
 - [12] E. Verhagen, S. Deleglise, S. Weis, A. Schliesser, and T. J. Kippenberg, *Nature* **482**, 63 (2012).
 - [13] M. Underwood, D. Mason, D. Lee, H. Xu, L. Jiang, A. B. Shkarin, K. Børkje, S. M. Girvin, and J. G. E. Harris, *Phys. Rev. A* **92**, 061801 (2015).

- [14] R. W. Peterson, T. P. Purdy, N. S. Kampel, R. W. Andrews, P.-L. Yu, K. W. Lehnert, and C. A. Regal, *Phys. Rev. Lett.* **116**, 063601 (2016).
- [15] W. H. P. Nielsen, Y. Tsaturyan, C. B. Møller, E. S. Polzik, and A. Schliesser, *Proceedings of the National Academy of Sciences* **114**, 62 (2017), <http://www.pnas.org/content/114/1/62.full.pdf>.
- [16] A. D. O'Connell, M. Hofheinz, M. Ansmann, R. C. Bialczak, M. Lenander, E. Lucero, M. Neeley, D. Sank, H. Wang, M. Weides, J. Wenner, J. M. Martinis, and A. N. Cleland, *Nature* **464**, 697 (2010).
- [17] T. Rocheleau, T. Ndukum, C. Macklin, J. B. Hertzberg, A. A. Clerk, and K. C. Schwab, *Nature* **463**, 72 (2010).
- [18] J. D. Teufel, T. Donner, D. Li, J. W. Harlow, M. S. Allman, K. Cicak, A. J. Sirois, J. D. Whittaker, K. W. Lehnert, and R. W. Simmonds, *Nature* **475**, 359 (2011).
- [19] T. A. Palomaki, J. W. Harlow, J. D. Teufel, R. W. Simmonds, and K. W. Lehnert, *Nature* **495**, 210 (2013).
- [20] A. P. Reed, K. H. Mayer, J. D. Teufel, L. D. Burkhardt, W. Pfaff, M. Reagor, L. Sletten, X. Ma, R. J. Schoelkopf, E. Knill, and K. W. Lehnert, *Nat Phys advance online publication*, (2017).
- [21] F. Massel, T. T. Heikkilä, J. M. Pirkkalainen, S. U. Cho, H. Saloniemi, P. J. Hakonen, and M. A. Sillanpää, *Nature* **480**, 351 (2011).
- [22] C. F. Ockeloen-Korppi, E. Damskäg, J.-M. Pirkkalainen, T. T. Heikkilä, F. Massel, and M. A. Sillanpää, *Phys. Rev. X* **6**, 041024 (2016).
- [23] L. D. Tóth, N. R. Bernier, A. Nunnenkamp, A. K. Feofanov, and T. J. Kippenberg, *ArXiv e-prints* (2016), arXiv:1602.05180 [quant-ph].
- [24] A. H. Safavi-Naeini and O. Painter, *New Journal of Physics* **13**, 013017 (2011).
- [25] C. A. Regal and K. W. Lehnert, *Journal of Physics: Conference Series* **264**, 012025 (2011).
- [26] J. M. Taylor, A. S. Sørensen, C. M. Marcus, and E. S. Polzik, *Phys. Rev. Lett.* **107**, 273601 (2011).
- [27] L. Tian, *Annalen der Physik* **527**, 1 (2015).
- [28] O. Černotík, S. Mahmoodian, and K. Hammerer, *ArXiv e-prints* (2017), arXiv:1707.03339 [quant-ph].
- [29] S. Barzanjeh, M. Abdi, G. J. Milburn, P. Tombesi, and D. Vitali, *Phys. Rev. Lett.* **109**, 130503 (2012).
- [30] Černotík, Ondřej and Hammerer, Klemens, *Phys. Rev. A* **94**, 012340 (2016).
- [31] A. M. Jayich, J. C. Sankey, B. M. Zwickl, C. Yang, J. D. Thompson, S. M. Girvin, A. A. Clerk, F. Marquardt, and J. G. E. Harris, *New Journal of Physics* **10**, 095008 (2008).
- [32] Q. P. Unterreithmeier, E. M. Weig, and J. P. Kotthaus, *Nature* **458**, 1001 (2009).
- [33] S. Schmid, T. Bağcı, E. Zeuthen, J. M. Taylor, P. K. Herring, M. C. Cassidy, C. M. Marcus, L. Guillermo Villanueva, B. Amato, A. Boisen, Y. Cheol Shin, J. Kong, A. S. Sørensen, K. Usami, and E. S. Polzik, *Journal of Applied Physics* **115**, 054513 (2014).
- [34] T. Bağcı, A. Simonsen, S. Schmid, L. G. Villanueva, E. Zeuthen, J. Appel, J. M. Taylor, A. Sørensen, K. Usami, A. Schliesser, and E. S. Polzik, *Nature* **507**, 81 (2014).
- [35] R. W. Andrews, R. W. Peterson, T. P. Purdy, K. Cicak, R. W. Simmonds, C. A. Regal, and K. W. Lehnert, *Nat Phys* **10**, 321 (2014).
- [36] A. Pitanti, J. M. Fink, A. H. Safavi-Naeini, J. T. Hill, C. U. Lei, A. Tredicucci, and O. Painter, *Opt. Express* **23**, 3196 (2015).
- [37] J. M. Fink, M. Kalae, A. Pitanti, R. Norte, L. Heinzle, M. Davanço, K. Srinivasan, and O. Painter, *Nature Communications* **7**, 12396 EP (2016).
- [38] T. Menke, P. S. Burns, A. P. Higginbotham, N. S. Kampel, R. W. Peterson, K. Cicak, R. W. Simmonds, C. A. Regal, and K. W. Lehnert, *ArXiv e-prints* (2017), arXiv:1703.06470 [quant-ph].
- [39] J. Bochmann, A. Vainsencher, D. D. Awschalom, and A. N. Cleland, *Nat Phys* **9**, 712 (2013).
- [40] A. Vainsencher, K. J. Satzinger, G. A. Peairs, and A. N. Cleland, *Applied Physics Letters* **109**, 033107 (2016), <http://dx.doi.org/10.1063/1.4955408>.
- [41] K. C. Balram, M. I. Davanço, J. D. Song, and K. Srinivasan, *Nat Photon* **10**, 346 (2016).
- [42] C.-L. Zou, X. Han, L. Jiang, and H. X. Tang, *Phys. Rev. A* **94**, 013812 (2016).
- [43] K. Takeda, K. Nagasaka, A. Noguchi, R. Yamazaki, Y. Nakamura, E. Iwase, J. M. Taylor, and K. Usami, *ArXiv e-prints* (2017), arXiv:1706.00532 [quant-ph].
- [44] R. L. Hudson and K. R. Parthasarathy, *Comm. Math. Phys.* **93**, 301 (1984).
- [45] C. W. Gardiner and M. J. Collett, *Phys. Rev. A* **31**, 3761 (1985).
- [46] B. Yurke and J. S. Denker, *Phys. Rev. A* **29**, 1419 (1984).
- [47] L. Lin, R. Howe, and A. Pisano, *Microelectromechanical Systems, Journal of* **7**, 286 (1998).
- [48] A. O'Connell and A. Cleland, "Microwave-frequency mechanical resonators operated in the quantum limit," in *Cavity Optomechanics*, edited by M. Aspelmeyer, T. J. Kippenberg, and F. Marquardt (Springer Berlin Heidelberg, 2014) pp. 253–281.
- [49] K. R. Brown, J. Britton, R. J. Epstein, J. Chiaverini, D. Leibfried, and D. J. Wineland, *Phys. Rev. Lett.* **99**, 137205 (2007).
- [50] C. W. Gardiner and P. Zoller, *Quantum Noise*, second enlarged edition ed., Springer series in synergetics, Vol. 56 (Springer, 2000).
- [51] V. Giovannetti and D. Vitali, *Phys. Rev. A* **63**, 023812 (2001).
- [52] F. Massel, S. U. Cho, J.-M. Pirkkalainen, P. J. Hakonen, T. T. Heikkilä, and M. A. Sillanpää, *Nat Commun* **3**, 987 (2012).
- [53] S. Schmid, C. Hierold, and A. Boisen, *Journal of Applied Physics* **107**, 054510 (2010).
- [54] X. Zhou, F. Hocke, A. Schliesser, A. Marx, H. Huebl, R. Gross, and T. J. Kippenberg, *Nat Phys* **9**, 179 (2013).
- [55] S. H. Crandall, D. C. Karnopp, J. Edward F. Kurtz, and D. C. Pridmore-Brown, *Dynamics of mechanical and electrome-*

chanical systems, edited by S. H. Crandall (McGraw-Hill, 1968).

- [56] F. Elste, S. M. Girvin, and A. A. Clerk, *Phys. Rev. Lett.* **102**, 207209 (2009).
- [57] A. Xuereb, C. Genes, and A. Dantan, *Phys. Rev. Lett.* **109**, 223601 (2012).
- [58] A. B. Shkarin, N. E. Flowers-Jacobs, S. W. Hoch, A. D. Kashkanova, C. Deutsch, J. Reichel, and J. G. E. Harris, *Phys. Rev. Lett.* **112**, 013602 (2014).
- [59] R. Dorf and J. Svoboda, “Introduction to electric circuits,” (John Wiley & Sons, 2010) Chap. 5 Circuit Theorems, 8th ed.
- [60] D. M. Pozar, *Microwave Engineering*, 4th ed. (John Wiley & Sons, Inc., 2012).
- [61] H. Nyquist, *Phys. Rev.* **32**, 110 (1928).
- [62] E. Zeuthen, A. Schliesser, A. S. Sørensen, and J. M. Taylor, ArXiv e-prints (2016), arXiv:1610.01099 [quant-ph].
- [63] S. Weis, R. Rivière, S. Deléglise, E. Gavartin, O. Arcizet, A. Schliesser, and T. J. Kippenberg, *Science* **330**, 1520 (2010), <http://www.sciencemag.org/content/330/6010/1520.full.pdf>.
- [64] A. H. Safavi-Naeini, J. Chan, J. T. Hill, S. Gröblacher, H. Miao, Y. Chen, M. Aspelmeyer, and O. Painter, *New Journal of Physics* **15**, 035007 (2013).
- [65] A. A. Clerk, M. H. Devoret, S. M. Girvin, F. Marquardt, and R. J. Schoelkopf, *Rev. Mod. Phys.* **82**, 1155 (2010).
- [66] A. H. Safavi-Naeini, S. Groblacher, J. T. Hill, J. Chan, M. Aspelmeyer, and O. Painter, *Nature* **500**, 185 (2013).
- [67] T. P. Purdy, P.-L. Yu, R. W. Peterson, N. S. Kampel, and C. A. Regal, *Phys. Rev. X* **3**, 031012 (2013).
- [68] A. I. Lvovsky, ArXiv e-prints (2014), arXiv:1401.4118 [quant-ph].
- [69] S. Mancini and P. Tombesi, *Phys. Rev. A* **49**, 4055 (1994).
- [70] C. Fabre, M. Pinard, S. Bourzeix, A. Heidmann, E. Giacobino, and S. Reynaud, *Phys. Rev. A* **49**, 1337 (1994).
- [71] J. M. Dobrindt, I. Wilson-Rae, and T. J. Kippenberg, *Phys. Rev. Lett.* **101**, 263602 (2008).
- [72] E. Zeuthen et al, in preparation.
- [73] Y.-D. Wang and A. A. Clerk, *Phys. Rev. Lett.* **108**, 153603 (2012).
- [74] L. Tian, *Phys. Rev. Lett.* **108**, 153604 (2012).
- [75] K. Stannigel, P. Rabl, A. S. Sørensen, P. Zoller, and M. D. Lukin, *Phys. Rev. Lett.* **105**, 220501 (2010).
- [76] G. Burkard, R. H. Koch, and D. P. DiVincenzo, *Phys. Rev. B* **69**, 064503 (2004).
- [77] G. Burkard, *Phys. Rev. B* **71**, 144511 (2005).
- [78] S. E. Nigg, H. Paik, B. Vlastakis, G. Kirchmair, S. Shankar, L. Frunzio, M. H. Devoret, R. J. Schoelkopf, and S. M. Girvin, *Phys. Rev. Lett.* **108**, 240502 (2012).